Structural inheritance and its control on overpressure preservation in mature sedimentary basins (Dongying depression, Bohai Bay Basin, China)

Ze Tao[1], Zhiliang He[2*], Tiago M. Alves[3], Xiaowen Guo[1], Sheng He[1], Wen Zhao[1]

[1] Key Laboratory of Tectonics and Petroleum Resources, Ministry of Education, China University of Geosciences, Wuhan, 430074, China

[2] Department of Science and Technology, China Petroleum & Chemical Corporation, Beijing, 100728, China

[3] 3D Seismic Lab – School of Earth and Ocean Sciences, Cardiff University – Park Place Cardiff, CF10 3AT, United Kingdom

Abstract

Overpressure in sedimentary basins has practical commercial importance for petroleum exploration, as the steady maintenance of pore pressure in reservoirs is important for CO_2 sequestration. Traps associated with faults comprise >30% of hydrocarbon discoveries in the Dongying depression, Bohai Bay Basin. However the way structural inheritance, together with fault reactivation and its development, influence pore-pressure development and overpressure preservation remain poorly understood. This research uses high-resolution 3D seismic data combined with well-log data to investigate the structural evolution in the Lijin and Boxing sags in the Dongying depression and elucidate the influence of structural inheritance on overpressure development. The interpreted data reveal that: 1) five fault families in the Lijin Sag influence overpressure development, 2) three phases of faulting occurred in the Boxing Sag during the syn-rift stage, with fault reactivation predominating in the early Eocene and late Oligocene; and 3) pressure coefficients (Pc) in Eocene strata vary from 0.90–1.96 in the Lijin and Boxing sags. In the Boxing Sag, Pc values vary from 0.91 to 1.54 in the Eocene strata, with 99% of overpressure coefficients below 1.50. In conparison, pressure coefficients in the Lijin Sag are significantly higher than in the Boxing Sag, with Pc values varying from 0.9 to 1.96, and 30% of the Pc values are over 1.50. This study concludes that inherited structures significantly control the development of overpressure in sedimentary basins. Systematic fault reactivation often leads to fluid leakage, which has a negative influence on overpressure preservation. In basins with border faults controlling their evolution, high-magnitude overpressure tends to be generated and maintained, favoring the formation of pressure compartments, conditions less ideal for carbon sequestration.

Keywords: Overpressure; Structural inheritance; Dongying depression, CO_2 sequestration

1. Introduction

Overpressure in sedimentary basins is a major geohazard, causing uncertainties in well planning and drilling (Osborne and Swarbrick, 1997; Dugan and Flemings, 2000; Moernaut et al., 2017). Overpressured intervals, or compartments, can be as shallow as a few hundred meters below the surface, or occur at depths exceeding 6 or 7 km, in strata ranging from the Precambrian to the Pleistocene (Serebryakov et al., 1995). Nevertheless, many of the world's largest oil and gas fields are associated with overpressured reservoirs (Hunt, 1990; Grauls and Baleix, 1994; Liu et al., 2017).

A number of mechanisms have been proposed to explain the generation of overpressure in sedimentary basins, among which disequilibrium compaction and fluid

expansion prevail in the published literature (Tingay et al., 2009; Guo et al., 2010; Tingay et al., 2013; Suwannasri et al., 2014; Liu et al., 2016; Wang et al., 2016; Raimbourg et al., 2017; Brüch et al., 2019). By definition, overpressured intervals are inherently unstable and tend to return to hydrostatic equilibrium after they are generated (Borge, 2002). Examples include shale reservoirs in which oil and gas are sourced and trapped within the same stratigraphic units. Hence, high-magnitude overpressure is assumed to occur only within or proximal to their origin, or sources (Swarbrick and Osborne, 1998; Bowker, 2007; Lee and Deming, 2002). However, reservoirs worldwide often comprise oil and gas from various sources, suggesting multiple mechanisms for generating overpressure within the same reservoir intervals. Overpressure transfer, laterally or vertically, has thus been proposed to contribute to high-magnitude overpressure intervals (Tingay et al., 2007; Yardley and Swarbrick, 2000). Yardley and Swarbrick (2000) have demonstrated that overpressure can be redistributed within inclined, isolated reservoirs, resulting in its "lateral transfer" onto structural crests. Research has also demonstrated that vertically transferred overpressure, via active faults and fractures, is capable of generating high-magnitude overpressure. Overburden unloading in tectonically inverted basins can also be an important process generating overpressure (Xiaorong et al., 2003; Tingay et al., 2007; Tingay et al., 2009; Luo et al., 2003).

Structural inheritance, as defined by Schiffer et al. (2020), is a property of the continental lithosphere that guides deformation along pre-existing rheological heterogeneities at all scales, which can impact the location, shape, and orientation of rift systems (Samsu et al., 2020; Schiffer et al., 2020; Wilson, 1966; Heron et al., 2019; Şengör et al., 2019) and smaller-scale faults within rift basins (Phillips et al., 2018; Reeve et al., 2015; Bertrand et al., 2018; Samsu et al., 2020; Wedmore et al., 2020). As summarized by Muñoz-Barrera et al. (2020), pre-existing structures can: a) be reactivated during extension or shortening, b) control the nucleation and localization of new faults during subsequent tectonic events; c) cause stress field perturbations and the formation of non-collinear fault networks; d) control the segmentation of faults and rift basins; e) influence the length, orientation, spacing, and evolution of faults; and f) control the shape and evolution of necking zones on rifted continental margins. When structural inheritance is prominent under a given stress field, fault reactivation and reworking represent the two primary mechanisms of deformation in sedimentary basins, pointing out to the repeated focusing of deformation along discrete pre-existing structures, with repeated focusing of metamorphism, ductile deformation, recrystallization, metasomatism, and magmatism into the same lithospheric volume (Schiffer et al., 2020). A common hypothesis suggests that basinal deformation is associated with the reactivation of inherited structures (Tarayoun et al., 2018), with structural inheritance being often considered to affect deformation at various scales (Tarayoun et al., 2018; Şengör et al., 2019; Muñoz-Barrera et al., 2020). This study refers to structural inheritance as: 1) fault reactivation, which results in faulting processes that are parallel to pre-existing structures, and 2) faults that are generated in shallower stratigraphic units, which are not directly linked to pre-existing faults but are influenced by the evolution of pre-existing structures. As indicated by Samsu et al. (2020), pre-existing basement structures exert a significant control on the orientation and distribution of faults and fractures in the sedimentary cover of a rift basin, but not always result in the generation of structures that are parallel to basement features (Samsu et al., 2020).

Structural inheritance and overpressure in sedimentary basins are inherently related to faults, and major fracture networks are significant in the transitory dynamics of fluid flow (Grauls and Baleix, 1994; Sibson, 1990). Faults represent the primary pathways by which fluids flow from deep reservoirs to the surface (Faulkner et al., 2010, Gunasekaran. et al., 2020),, but can also act locally as impermeable barriers (Frery et al., 2015). The reactivation may influence the complexity of faults, fractures, and folds at kilometer scales and smaller, leading to fluid escape and retention episodes. Therefore, reactivation will significantly impact the development of geological structures at all scales,

and their pressure histories, including the location and nature of fluid transference, trap geometries, and reservoir performance (Holdsworth, 2017; Wiprut and Zoback, 2000).

Apart from the importance of structural inheritance on fluid dynamics in sedimentary basins, understanding how structural inheritance can potentially influence overpressure development and maintenance in mature exploration basins is vital in carbon sequestration (Bachu, 2016). Emissions from stationary facilities, such as fossil fuel power plants, steel plants, refineries, and cement plants, can be captured, compressed, and injected into underground rock formations (e.g., into oil reservoirs) where the caprock can prevent the injected fluid from escaping to the surface (Bachu, 2016). Depleted oil reservoirs are ideal geological sites for CO_2 storage, and injecting CO_2 into mature oilfields for enhanced oil recovery is an effective method for reducing CO_2 emissions. Moreover, the cost of CO_2 storage is reduced in geological traps of oil fields that have previously stored substantial volumes of hydrocarbons, including natural gas (Gunasekaran. et al., 2020, Li and Li, 2017).

The Bohai Bay Basin is the largest, most prolific petroliferous basin in China, where the majority of oil reservoirs have been water flooded and produced high water-cuts for decades (Yang et al., 2017). In the broader Bohai Bay, CO_2-EOR technology is a useful method to enhance oil recovery. As predicted by Yang et al. (2017), 683 million tons (Mt) of additional oil may be produced from candidate oil reservoirs after applying CO_2-EOR techniques, and 1,345 Mt of gaseous CO_2 can simultaneously be stored in these same Eocene reservoirs in the Shahejie Formation (Es_3 and Es_4). In order to understand overpressure development in this mature petroleum basin, and its relationship with structural inheritance, this study aims to:

1) Document the multiple fault systems developed in different sub-basins of the Dongying depression, i.e. the Lijin and Boxing Sags;
2) Understand different structural inheritance mechanisms in the Lijin and Boxing sags;
3) Analyze present-day pore pressure development in the two sags, and their relationship with structural inheritance;
4) Characterize the relationship between structural inheritance and safe CO_2 sequestration.

2. Geological background

The Bohai Bay Basin is a large Mesozoic–Cenozoic continental rift basin comprising substantial petroleum reserves, covering an area of approximately 200,000 km^2 in East China (Guo et al., 2010; Li et al., 2012; Qiu et al., 2015; Li et al., 2017; Feng et al., 2013) (Fig. 1). The Bohai Bay Basin experienced four main tectonic phases since the middle Proterozoic: 1) tectonic stability and sedimentation from the middle-late Proterozoic to the end of the Paleozoic (Li et al., 2017), 2) continuous uplift and folding during the Mesozoic, following the onset of Hercynian tectonism in the late Permian, 3) continental rifting due to the subduction of the Pacific Plate beneath the Eurasian Plate, and consequent upwelling of mantle from the Late Jurassic to Early Cretaceous, and 4) thermal subsidence after the Late Cretaceous. At present, the boundaries of the Bohai Bay Basin constitute a series of normal faults recording multiple episodes of movement (Allen et al., 1997; Hsiao et al., 2004), associated with distinct phases of rifting and subsidence during the Cenozoic (Allen et al., 1997), and subduction rollback of the Pacific plate relative to the eastern margin of Asia (Allen et al., 1997; Watson et al., 1987; Feng et al., 2013) (Fig. 2).

The Bohai Bay Basin comprises seven sub-basins, or sags: the Liaohe, Liaodong, Bozhong, Jiyang, Huanghua, Jizhong, and Linqing sags (Allen et al., 1997) (Fig. 1a). In addition, the Dongying depression is a NEE-trending rift lacustrine basin located in the Jiyang Sag, which is one of the most prolific hydrocarbon-rich areas of the Bohai Bay Basin (You et al., 2020, Zahid et al., 2016) (Fig. 1a). The depression is bounded by the Chenjiazhuang Rise, Qingtuozi Rise, Luxi Uplift, Guangrao Rise, and the Qingcheng Rise (Fig. 1b), and reveals an asymmetric geometry with a steeply dipping northern part and a gently sloping southern part (Zhang et al., 2009) (Figs.

1b and 2). Five structural zones are identified in the depression: the northern steep slope zone, the Lijin Sag, the central diapiric anticline zone, the Niuzhuang Sag, and the southern gentle slope (Liu et al., 2017). The Boxing, Niuzhuang, Lijin, and Minfeng sags cover an exploration area of approximately 5700 km^2 in the larger Dongying depression (Wang et al., 2016) (Fig. 1b).

The structural evolution of the Dongying depression can be divided into three primary stages: 1) formation, deformation, and consolidation of the platform basement from the Archean to the early–middle Proterozoic, 2) stable platform development from the late Proterozoic to Paleozoic, and 3) rift-basin development in the Cenozoic. The Dongying depression is generally regarded as a Cenozoic fault-bounded depression that resulted from continental rifting (Wang et al., 2016; Wang et al., 2020). The Paleocene records the main syn-rift stage (65.0–24.6 Ma) while the post-rift stage spans 24.6 Ma to the present-day (Hu et al., 2001). The Paleogene syn-rift stage can be further divided into four tectonic episodes: 1) initial rifting from the Paleocene to early Eocene (65–50.4 Ma), 2) rifting in the Middle Eocene (50.4–42.5 Ma), 3) rift climax from the late Eocene to early Oligocene (42.5–38 Ma), and 4) late rifting during the Oligocene (38–24.6 Ma) (Fig. 3). Faults developed in the Bohai Bay Basin were classified into distinct orders, with the Tanlu Fault streching over 2400 km and offseting the continental crust, thus comprising the main 1st-order fault in the study area. Faults with smaller scales, which propagate 10s of kilometers onto low velocity zones in the crust are 2nd-order faults, and significantly influenced the evolution of distinct sags in the Bohai Bay Basin (Fig. 2). According to Dou et al. (2020) the Shengtuo Fault, offsetting the basement in the Dongying depression, comprises a 3rd-order fault and greatly controls the development of fault systems in the Lijin Sag (Fig. 4).

The strata filling the Dongying depression are grouped in the Paleozoic Kongdian (Ek), Shahejie (Es), and Dongying (Ed) formations, the Neogene Guantao (Ng) and Mighuazhen (Nm) formations, and the Quaternary Pingyuan (Qp) Formation (Fig. 3). A regional unconformity at the end of the Oligocene separates the syn- and post-rift units and coincides with the boundary between the Ed and Ng formations (Zahid et al., 2016) (H6 in Fig. 3). In the early evolution stages of the Dongying depression, an unconformity was also developed between the Es3 and Es4 members of the Paleogene Shahejie Formation (H3 in Fig. 3).

The Kongdian Formation comprises shale and siltstone with intercalated sandstone and volcanics (Fig. 3). During the deposition of the Es_4 member, the Dongying depression was predominantly a lacustrine environment (Zahid et al., 2016), hosting organic-rich black shale reaching 200 m in thickness (Fig. 3). The lowest part of the Shahejie Formation (the Es_4 member) consists of layers of red sandstone and mudstone interbedded with evaporite deposits (Fig. 3). The depositional environment shifted from lacustrine during stage 2 rifting to a semi-deep lake during stage 3 (rift climax). Consequently, the Es_3 member is composed of gray mudstone, oil shale intercalated with sandstones, and thin layers of limestone (Feng et al., 2013). Stage 4 (late rifting) resulted in a shallower water body, with deposits of the Es_2 and Es_1 members comprising mudstone, sandstone, and siltstone intercalated with coarse sand conglomerates and biogenic carbonates (Fig. 3). The Late Oligocene Dongying Formation (Ed) comprises coarse sandstone and medium to fine sandstones interbedded with gray mudstones (Fig. 3). Post-rift sediments (24.6 Ma to Recent) include sandstone and siltstones interbedded with transgressive mudstones (Fig. 3).

Paleogene syn-rift strata comprise the major hydrocarbon source rocks and reservoir rocks in the Dongying depression (Allen et al., 1997). According to previous studies, there are three sets of main hydrocarbon source intervals in the Paleogene Shahejie Formation: the upper Es_4, the lower Es_3, and the upper Es_3 members (Song et al., 2020, Zhang et al., 2009) (Fig. 3). Intercalated sandstone and siltstones in the Es_4 and Es_3 members comprise the main reservoirs in the Dongying depression, and overpressure is widely developed throughout the study area (Guo et al., 2016; Guqiang et al., 2003; Wang et al., 2010).

3. Data and methods

Two seismic volumes from the Dongying depression, Bohai Bay Basin, were interpreted in this study (Fig. 1b). Interpreted 3D seismic data in the Lijin Sag covers an area of approximately 1600 km^2, with a sampling interval of 4 ms, and a bin spacing of 25 m × 25 m. Vertical resolution can reach 20 m near the surface and reaches 40 m at the depth of strata investigated in this work. The 3D seismic volume from the Boxing Sag covers an area of 1800 km^2, with a sampling interval of 2 ms and a bin spacing of 25 m × 25 m. Seismic interpretation was completed using Schlumberger's Petrel®, and seven regional stratigraphic horizons were interpreted in this work (Fig. 3). The relative ages of the interpreted seismic units were taken from the published literature (Su et al., 2011; Li et al., 2012), and are consistent with the stratigraphic framework of Sinopec's Exploration and Production Research Institute. Key stratigraphic markers include: 1) a Paleocene and Eocene interface (horizon H1) marking the boundary between syn-rift stages 1 and 2; 2) the base of the Es3 member (horizon H3), representing the boundary between syn-rift stages 3 and 4; 3) the top of the Es3 member (horizon Hx), which marks the shift from a relatively deep lake to a shallow-lake depositional environment; and 4) the Oligocene and Miocene horizon Hx, a regional unconformity marking the boundary between syn-rift and post-rift tectonics in the study area (Feng et al., 2013) (Fig. 3).

Seismic interpretation, the detailed mapping of key horizons and faults, and variance maps, were used to understand fault development and their hierarchy (Figs. 4 to 7). In parallel, throw-depth (T-Z) were compiled following the principle proposed by Tao and Alves (2019) in which throw data should be collected above certain limits in resolution to minimize data uncertainty. T-Z profiles are comprehensively used in industry and academia to analyse fault reactivation and associated tectonic movements (Baudon and Cartwright, 2008a; Baudon and Cartwright, 2008b; Baudon and Cartwright, 2008c; Tao and Alves, 2016) (Fig. 8).

Borehole data were used to identify the locations where overpressure has developed (Fig. 1b). In total, seven (7) wells in the Lijin Sag and 11 wells in the Boxing sag were tied to the available seismic data (Figs. 1b, 9, and 10). In this work, a seismic-well tie was completed near Well T719, Lijin Sag, as an example of how to accurately measure overpressure using a combination of borehole a seismic data (Fig. 9). In this work, overpressure magnitude is defined as low, moderate, and high based on Pc thresholds of $1.1 < Pc < 1.2$, $1.2 < Pc < 1.5$, and $Pc > 1.5$, respectively. Conversely, Pc values between 0.9 and 1.1 are regarded as hydrostatic owing to testing uncertainties (Guqiang et al., 2003). Pore-pressure coefficients derived directly from logging-while-drilling (LWD) data were used to understand the overall pore pressure development in the Es_4 and Es_3 members. This work used data from 85 wells from the Lijin Sag and 120 wells from the Boxing Sag for this latter purpose (Fig. 11).

4. Faults developed in the Lijin and Boxing sags

The Boxing and Lijin sags record a similar tectonic evolution since the Paleocene (Feng et al., 2013; Allen et al., 1997) (Fig. 1). However, faults developed in these two sags vary in terms of their evolution and geometries (Figs. 4–7).

4.1 Fault families in the Lijin Sag

According to Dou et al. (2020), the formation of faults in the Dongying depression was mainly controlled by the combined effects of dextral strike-slip movements and NW–SE tensile stresses. Consequently, a third-order large-scale normal fault - the Shengtuo Fault - was developed in an E–W direction (Figs. 4 and 5). The Shenguo Fault controlled the formation and evolution of the Dongying depression (Dou et al., 2020, Chen et al., 2017).

Five fault families were identified in the Lijin Sag. Family 1 is best represented by the Shengtuo Fault, which strikes E–W and offsets the basement in the Lijin Sag (Figs. 4 and 5). Family 2 represents faults formed during the syn-rift stage 1, and offset the Paleocene Kongdian Formation (Fig. 4). Family 3 includes faults developed during syn-rift stage 3 (between

horizons H2 and H3), that offset overlying (younger) strata during subsequent reactivation stages (Figs. 4 and 5). Family 4 comprises tier-bound faults developed during syn-rift stage 3 in strata delimited by horizons H3 and H4. Family 5 faults were formed during the post-rift stage and document maximum throw values at horizon H6 (Figs. 4, 5 and 8).

Figure 4 shows a representative seismic profile with the five families of faults identified in the Lijin Sag (Fig. 4). The Shengtuo Fault is the largest fault in the study area and is regarded as a 3rd-order fault in the Bohai Bay Basin extending from basement rocks to the surface (Fig. 4). The hanging-wall block of the Shengtuo Fault is the main depocenter of the Lijin Sag (Fig. 4). On its footwall block, only thin syn-rift strata were preserved (~1000 ms two-way time (twt) but a thickness of over 3000 ms twt strata is observed in its adjacent hanging-wall depocenter (Fig. 4). The maximum throw of the Shengtuo Fault reaches 1427 ms twt (Fig 4).

During syn-rift stage 1, intensive rifting led to normal faulting in the Bohai Bay Basin, generating normal faults in Family 2 (Fig. 4). As observed from the interpreted seismic profiles and variance maps in Figs. 4 and 5d, faults developed during syn-rift stage 1 did not propagate into younger strata, forming a fault family that had limited influence on subsequent faults (Figs. 4 and 5d). Faults in Family 3 strike E–W and offset syn-rift stage 2 and post-rift strata (Fig. 5). Fault Family 4 comprises a group of tier-bound faults bounded by horizons H3 and H4 (Fig. 4). Strata bounded by H3 and H4 comprise sandstone and siltstone reservoirs in the Lijin Sag (Fig. 3). Fault Family 5 has lower tips terminating at horizon H4, with faults propagating to the surface (Fig. 4). From the variance maps, Fault Families 4 and 5 are separated by the Es_1 member. The Es_1 member comprises mudstones, showing strong and continuous reflections on seismic data. This lithology may play a part in forming local detachments between syn-rift stage 4 and post-rift strata (Figs. 3, 4, 5a, and 5b).

4.2 Inherited faults and fault reactivation in the Boxing Sag

Faults in the Boxing Sag developed during syn-rift stages 1 and 2, below horizon H2 in Fig. 6, and were inherited from pre-existing faults to offset younger strata (Fig. 6), These faults differ from those developed in the Lijin Sag, where fault families developed only in distinct stratigraphic units (Fig. 4). Importantly, the Shengtuo Fault in the Lijin Sag comprises a 3rd-order fault (Fig. 4) and is regarded as a basin-shoulder, or border, fault. In the Boxing Sag, 3rd-order faults do not occur, highlighting a key difference between the two sags (Fig. 6). Instead, the variance maps in Fig. 7 reveals densely distributed faults at all stratigraphic levels.

4.2.1 Main episodes of faulting

Based on the interpreted seismic data, three episodes of faulting in the Boxing Sag are identified as follows: phase 1 faults, reflecting faulting during syn-rift stages 1 and 2 (they span the basement to horizon H2); phase 2 faults, marking the reactivation of phase 1 faults; and later fault propagation and reactivation at the level of horizon H6 (Fig. 6). Intensive faulting occurred in the Bohai Bay Basin during syn-rift stages 1 and 2, while densely conjugate faults were formed in the Boxing Sag (Figs. 6 and 7c). A regional unconformity (horizon H2) was later developed throughout the study area, and reflects significant erosion in the Boxing Sag (Fig. 6).

Most faults formed during syn-rift stages 3 and 4 were inherited from faults generated in phase 1. Consequently, fault dips and strikes are similar between horizons H2 and H6 (Figs. 6 and 7). The seismic data show that some inherited and reactivated faults terminate at H6 or below (Fig. 6). When comparing variance maps below and above horizon H6, some faults developed below horizon H6 (Fig. 7b) are not visible above this same seismic-stratigraphic marker (Fig. 7a). Hence horizon H6, a regional unconformity formed at the end of the Oligocene (Fig. 3), comprises the stratigraphic boundary marking the end of syn-rift stage 3 faulting in the Boxing Sag, where further fault propagation and reactivation did not occur above this horizon (Fig. 6). Please, check if the re-phrasing of this sentence is the correct.

4.2.2 *Fault reactivation estimated from Throw-Depth (T-Z) plots*

To better understand fault evolution in the Boxing sag, five faults (i.e., B1, B2, B3, B4, and B6), offsetting horizons H2 and H6, were selected to compile T-Z plots (Fig. 8). The five faults record increases in throw values at horizon H2 or below, a character materialising faulting during syn-rift stages 1 and 2 (Fig. 8). Four of the faults reveal two reactivation episodes, except for fault B4 with only one phase of fault reactivation (Fig. 8). In faults B1 and B2, the second phase of fault reactivation occurred at horizon H6, where throw minima are observed and throws above horizon H6 are relatively smaller than below (Fig. 8). In fault B3, fault reactivation occurred at the level of horizon H7, marking a later stage of fault reactivation (Fig. 8). Faults B4 and B6 reveal their second reactivation episode at horizon H4, which marks the boundary between syn-rift phases 3 and 4 (Figs. 3 and 8).

The results of the T-Z plot analysis support the assumption that three phases of faulting occurred in the Boxing Sag, and were separated by two regional unconformities: horizons H2 and H6 (Figs. 6 and 8). However, intense fault reactivation observed in seismic data indicates that the reactivation of some faults may also have occurred during syn-rift stage 4 (e.g., faults B4 and B6 in Fig. 8) and during the post-rift stage (e.g., fault B3 in Fig. 8).

5. Basin overpressure

Representative seismic profiles, tied to borehole data, were analyzed to plot measured overpressure values in the Lijin and Boxing sags (Figs. 9 and 10). Seismic profiles intersected seven (7) wells in the Lijin Sag and 11 wells in the Boxing Sag (Figs. 1b, 9, and 10). Pressure coefficients (Pc) were calculated from LWD data in the main reservoir intervals (Es_3 and Es_4 members) (Fig. 11). In total, 85 wells in the Lijin Sag and 120 wells in the Boxing Sag were used in this work (Fig. 11).

5.1 *Pressure coefficients in the Es_3 and Es_4 members*

5.1.1 *Lijin Sag*

The pressure coefficients in the Es4 member were estimated based on three wells drilled in the Lijin Sag, T140, T719, and T710, while four wells (T714, T 712, T71, and T711) were used to calculate Pc in the Es_3 member (Fig. 9).

In the Es_4 member, the pressure coefficient at well T140 is 1.77, which is categorized as a high overpressure (Fig. 9). In wells T719 and T710, pressure coefficients are 1.19, and 1.29, respectively, correlating with low to moderate overpressures (Fig. 9). Apart from a normal pressure coefficient of 0.85 in well T711 within the Es_3 member, other wells document high overpressure in Es_3, with pressure coefficients of 1.70 in well T714, 1.68 in well T712, and 1.86 in well T71 (Fig. 9).

Pore pressure declines significantly when approaching Fault L1, which offsets the basement and strata above (Fig. 9). High overpressure develops on the hanging-wall block of L1 in both Es_3 and Es_4 members (Fig 9). Only low to moderate overpressure is developed on the footwall block of Fault L1, and also close to it. Normal pressure is recorded in well T711, which is the closest well to Fault L1, being located on its immediate hanging wall (Fig. 9).

5.1.2 *Boxing Sag*

Pressure coefficients for seven (7) wells in the Boxing Sag were documented in the Es_4 member. Four (4) other wells document overpressure in the Es_3 member (Fig. 10). In the Es4 member, a normal pore pressure of 1.09 is observed in well Tg85, located on the hanging wall of Fault B3 (Fig. 10). High overpressure is developed in well L109, documenting a pressure coefficient of 1.54 (Fig. 10). Other wells show low to moderate overpressure in the Es_4 member, with pressure coefficients of 1.26 in well Tg81, 1.14 in well Ch97, 1.33 in well Ch96, 1.26 in well Ch69, and 1.18 in well L5 (Fig. 10).

In the Es_3 member, wells Ch60 and Ch38 show normal pore pressure with coefficients of 0.95 and 1.09, respectively (Fig. 10). Wells Ch106 and Tg84 document moderate overpressure in the Es_3 member (Fig. 10).

5.2 Overpressure in the Es_3 and Es_4 members of the Lijin and Boxing sags

The LWD pore pressure data reveal that the pressure coefficient varies from 0.90 to 1.92 in the Lijin Sag, with 36 wells showing normal pore pressures, 28 wells presenting low to moderate pore pressures, and 26 wells recording strong overpressure in the Es_3 and Es_4 members (Fig. 11a). In the Boxing Sag, overpressure coefficients vary from 0.91 to 1.54. The results in this work show that, in the Es_4 member, 31 wells currently record normal pore pressure, 81 wells have low to moderate overpressure, and only one well shows a high pressure coefficient of 1.54 (Fig. 11a). Statistical data prove that overpressure was developed throughout the Lijin Sag, while weak to moderate overpressure was developed in the Boxing Sag, with high overpressures being rare and occurring only locally (Fig. 11a).

Overpressure distribution in the Es_3 and Es_4 members point to two distinct pressure compartments, both comprising two separate exploration targets in the Dongying depression (Li, 2004; Guqiang et al., 2003; Guo et al., 2010). To understand the magnitude of the overpressure in these two compartments, pressure coefficient data further discriminated between the Es_3 and Es_4 members (Figs. 11b and c). Results show that 16 wells with normal pore pressure, nine (9) wells with low overpressure, and 58 wells with moderate overpressure were tested in the Es_4 member in the Boxing Sag (Fig. 11b). Low to moderate overpressure characterizes the Es_4 member of the Boxing Sag (Fig. 11b). In the Es_4 member of the Lijin Sag, 10 wells exhibit normal pore pressure, nine (9) wells record moderate pressure, and 11 wells have high pressure coefficients (Fig. 10). These data prove that moderate to high overpressures describe the overall pressure conditions in the Es4 member of the Lijin Sag (Fig. 11b).

The pore pressures in the Es_3 member in the Lijin and Boxing Sags show similar patterns; low to moderate overpressure was observed in the Boxing Sag in 6 out of 14 wells, while 28 out of 47 wells showed moderate to high overpressure in the Lijin Sag (Fig. 11c).

6. Discussion

~~7.1~~6.1 Structural inheritance controlled by basin-shoulder faults

The Dongying depression is surrounded by raised Precambrian basement blocks bounded by normal faults (Feng et al., 2013; Allen et al., 1997; Ren et al., 2002). The Shengtuo Fault comprises a 3rd-order fault in the Bohai Bay Basin controlling the structural evolution and sedimentation in the Lijin Sag, and is regarded as a basin-shoulder, or border, fault (Dou et al., 2020). Border faults were first identified in rift basins forming prominent fault escarpments on their shoulders; they have large displacements and lengths due to accommodating the bulk of strain and stress in extensional settings (Crossley and Crow, 1980; Ebinger et al., 1987). This structural control occurs at different scales of analysis; in the Espírito Santo Basin, SE Brazil, Ze and Alves (2016) proposed that fault families developed on the crest of salt structures were controlled by border faults, which have the largest maximum throws and accommodate most of the strain and stress on the crest of salt structures. Faults close to border faults are often less active, and are in a less preferential position to propagate and reactivate. this, border faults often impact the location, shape, and orientation of rift systems, and associated smaller faults development (Schiffer et al., 2020; Wedmore et al., 2020).

In the Lijin Sag, the Shengtuo Fault has a maximum throw of 1427 ms twt (conversion to metres here), a value significantly higher than any other fault in the study area (Fig. 4). From the variance maps, the Shengtuo Fault is also the longest when compared to other faults developed in the multiple stratigraphic units identified in seismic and borehole data (Fig. 5). The Shengtuo Fault is currently an active fault with surface expression (Fig. 4).

Fault families in the Lijin Sag were bounded by key stratigraphic units that, and include: 1) faults formed during syn-rift stages 1 and 2 (Family 2), which seldom propagate into the overlying strata (Figs. 4 and 5), and 2) faults formed during late syn-rift stage 3, comprising a

tier-bounded fault family. Only a few faults formed at this stage propagated into younger strata above (Families 3 and 4) (Figs. 4 and 5). The observation that multiple fault families were not reactivated during syn-rift stages 2 and 3 indicates that the Shengtuo Fault accommodated the bulk of strain and stress in the Lijin Sag during syn-rift, accumulating displacement and, consequently, smaller faults in the sag were not reactivated (Ze and Alves, 2016; Crossley and Crow, 1980; Ebinger et al., 1987). Family 5 faults formed during the post-rift stage (Fig. 4). During the late Oligocene, tectonic quiescence and a long period of denudation in the Lijin Sag led to the formation of a regional unconformity between syn-rift and post-rift strata (horizon H6 in Fig. 3). Post-rift tectonics resulted in the reactivation of the Shengtuo Fault, together with the formation of Family 5 faults during the post-rift stage (Fig. 4).

The Boxing Sag has faults developed in all stratigraphic units, and no fault stands out as comprising a border fault (Figs. 6 and 7). Instead, fault reactivation prevailed throughout the syn-rift and post-rift stages (Figs. 6 and 8). Three main phases of faulting were identified in the Boxing Sag (Fig. 6). The first phase recorded intensive faulting during syn-rift stages 1 and 2, with latter faulting phases reactivating stage 1 faults (Figs. 6 and 7). Other fault reactivation periods were also identified, as indicated by the T-Z analysis of distinct faults (Fig. 8). The T-Z analysis of fault B3 indicates that some faults were reactivated at the level of horizon H7, while analysis of fault B4 shows that fault reactivation occurred between syn-rift stages 3 and 4 (H4 in Fig. 8). The main period of fault reactivation in both the Lijin and Boxing sags correlate with synrift stage 2 and the transition between the synrift and postrift stages (Figs. 3, 4 and 8).

Different faulting processes in the Lijin and Boxing sags indicate that border faults exert significant control on structural inheritance, i.e., on fault reactivation and the generation of new faults. Strain was mainly accommodated by border fault(s) after their establishment, while other faults in sedimentary basins were inactive or remained quiescent (Fig. 4). In basins where no border faults are developed, fault reactivation dominates i.e., faulting in younger strata often results from the reactivation of pre-existing faults (Fig. 6).

Our findings suggest two end members explaining faulting in sedimentary basins: one controlled by border faults, and one where border faults are not important features accommodating stress and strain.

~~7.2~~6.2 *Structural inheritance and overpressure in sedimentary basins: Implications for CO_2 sequestration*

Figure 12 summarizes the structural evolution in the Lijin and Boxing sags as examples of two end-member faulting styles in sedimentary basins, and their control on overpressure development. In the first phase, the studied sags experienced widespread rifting during syn-rift stages 1 and 2, and multiple faults were formed (Fig. 12a and 12a'). In the Lijin Sag, a Cambrian basement feature led to the formation of the Shengtuo Fault, which was established as a border fault during stage 2 (Fig. 12b) (Dou et al., 2020). Few new faults formed in younger strata (Fig. 12b). Conversely, in the Boxing Sag fault reactivation dominated in younger strata, and no structures stand out as border faults (Fig. 12b').

With continuous sedimentation, shales and mudstones reached the depths in which oil can be generated, leading to the generation of local overpressure in both sags (Figs. 12c and 12c') (Guo et al., 2010). In the Lijin Sag, new faults were generated in younger strata, and these were not linked to faults formed during stage 1 (Fig. 12c). Fluid leakage along border faults and newly generated faults occurred this sag (Figs. 4 and 12c). In the Boxing Sag, a new phase of fault reactivation occurred, leading to the systematic release of fluid from source and reservoir intervals into younger strata or the surface, close to which pore pressure declines significantly more than that in the Lijin Sag (Fig. X).

New faults were generated in the Lijin Sag during the post-rift stage, and these were not linked with faults formed during syn-rift tectonics, i.e. the main petroleum system (bounded by horizons H1 and H4) was not faulted (Fig. 12d). Continuous oil and gas

generation led to an increase in pore pressure in the main hydrocarbon-rich units of the Lijin Sag. In the Boxing Sag, post-rift faults result from the reactivation of pre-existing structures. Faults at all stratigraphic units were reactivated, leading to further pore pressure decline in key reservoir intervals (Figs. 10 and 12d').

Our model is supported by present-day overpressure data for both sags (Figs. 9, 10, and 11). In the Lijin Sag, moderate to high overpressures are observed (Figs. 9 and 11). Pore pressures on the footwall block of fault L1, which offset the Es_3 and Es_4 members, and those close to this same fault, were significantly lower than on the hanging wall of L1 (Fig. 9). This indicates that faults were main fluid conduits in the Lijin Sag. Apart from fluid leakage along fault L1, the geometry of strata also contributes to the high pressure magnitude on the hanging-wall block; hanging-wall strata were flattened towards fault L1, while the footwall sequences favor updip fluid transfer towards fault L1 (Fig. 9). Owing to the development of border faults such as the Shengtuo Fault, other fault groups in the Lijin Sag remained quiescent, becoming inactive soon after they were formed. This favored the formation of fluid compartments and subsequent increases in pore pressure due to oil and gas generation.

In the Boxing Sag, weak to moderate overpressures developed in the Es_3 and Es_4 members (Figs. 10 and 11). The reactivation of various faults during discrete tectonic events (Fig. 8) in the Boxing Sag led to the significant release of fluids from reservoirs along reactivated faults, resulting in significant drops in pore pressure (Figs. 10 and 12). Nevertheless, some reactivated faults may still function as seals, such as Fault B6, where overpressure was developed in well L109 (Fig. 10). On the footwall of Faults B4 and B5, moderate overpressures were developed in wells Ch96, Ch69, and Ch106 (Fig. 10).

Geological traps of oil fields have been proven as potential CO_2 sequestration sites, and enhanced oil recovery via the injection of CO_2 (CO_2-EOR) in the Bohai Bay Basin has been deployed over a decade (Li et al., 2009; Li and Li, 2017; Bachu, 2016). The Eocene Shahejie Formations, inluding the Es_3 and Es_4 members, comprise important reservoirs in the Bohai Bay Basin, where gaseous CO_2 is systematically deployed to enhance oil recovery (e.g., Yang et al., 2017). The result of structural inheritance and its influence on overpressure development in sedimentary basins indicate that carbon sequestration in basins with border fault(s) may be safer than in basins without border faults. In fact, the systematic reactivation of faults in basins without border faults creates significant uncertainties for safe CO_2 sequestration. In our study we suggest that moderate-strong overpressures were preserved due to the existence of the Shengtuo Fault, which acts as a border fault controlling fault evolution in the Lijin Sag (Figs. 4, 9 and 13). Fault seal behaviour, unbreached seal units, and strata geometry, all contribute to the maintenance of overpressure compartments near border faults (Figs. 4, 9 and 13). Fluid injected in depleted oil and gas reservoirs near border faults are often more effective if these border faults are sealing structures. Conversely, basins with no border faults record systematic fault reactivation during successive tectonic events, leading to the generation of faulted, segmented reservoir units (Figs. 6 and 9). Breaching of seal units by reactivated fault systems often leads to seal failure and loss of pressure efficiency in reservoirs, a potential risk for safe CO_2 sequestration.

~~8.~~7. Conclusions

The detailed analysis of fault evolution and overpressure development in the Lijin and Boxing sags, Dongying depression, indicates that structural inheritance, namely the formation of border faults and subsequent fault reactivation, in a key control on overpressure development in sedimentary basins. The following conclusions were drawn from our findings:

1) Five fault families were developed in the Lijin Sag, with border faults controlling their evolution. Faults families were not linked in this basin. In the Boxing Sag, the reactivation of pre-existing faults occurred in multiple basin evolution stages. Two end-member faulting models in sedimentary basins are proposed in this work and differentiated by

the establishment of border faults.

2) Overall pore pressure in the Lijin Sag was higher than in the Boxing Sag. Moderate to high overpressure occurs widely in the Lijin Sag, while in the Boxing Sag weak to moderate overpressure characterizes the present-day conditions.
3) Fluid migration mainly occurs along the latter border faults, favoring the generation of strong overpressures. In basins without border faults, systematic fault reactivation during successive stages leads to a decline in pore pressure and the formation of fluid compartments.
4) Of the two end members of faulting in sedimentary basins, basins with significant border faults are relatively safer for CO2 sequestration (the Lijin type) compared to basins without border faults (the Boxing type).

Further regional tectonics may facilitate systematic fault reactivation in basins without border faults, bringing greater risks in terms of CO_2 sequestration.

Acknowledgements

The authors thank Dr. Davide Gamboa for his constructive and insightful comments, which greatly improve the paper. The Shengli Oil Field, Sinopec is acknowledged for the seismic and well data used in this research. Schlumberger is acknowledged for the provision of data interpretation software. The authors acknowledge funding from the National Natural Science Foundation of China (Project No. 41902198, No. U20B6001) and the China postdoctoral Science foundation (Project No. 2019M662738).

References

ALLEN, M. B., MACDONALD, D. I. M., XUN, Z., VINCENT, S. J. & BROUET-MENZIES, C. 1997. Early Cenozoic two-phase extension and late Cenozoic thermal subsidence and inversion of the Bohai Basin, northern China. *Marine and Petroleum Geology,* 14**,** 951-972.

BACHU, S. 2016. Identification of oil reservoirs suitable for CO 2 -EOR and CO 2 storage (CCUS) using reserves databases, with application to Alberta, Canada. *International Journal of Greenhouse Gas Control,* 44**,** 152-165.

BARNETT, J. A., MORTIMER, J., RIPPON, J. H., WALSH, J. J. & WATTERSON, J. 1987. Displacement geometry in the volume containing a single normal fault. *AAPG Bulletin,* 71**,** 925-937.

BAUDON, C. & CARTWRIGHT, J. 2008a. 3D seismic characterisation of an array of blind normal faults in the Levant Basin, Eastern Mediterranean. *J. Struct. Geol.,* 30**,** 746-760.

BAUDON, C. & CARTWRIGHT, J. 2008b. Early stage evolution of growth faults: 3D seismic insights from the Levant Basin, Eastern Mediterranean. *Journal of Structural Geology,* 30**,** 888-898.

BAUDON, C. & CARTWRIGHT, J. 2008c. The kinematics of reactivation of normal faults using high resolution throw mapping. *Journal of Structural Geology,* 30**,** 1072-1084.

BERTRAND, L., JUSSEAUME, J., GéRAUD, Y., DIRAISON, M., DAMY, P.-C., NAVELOT, V. & HAFFEN, S. 2018. Structural heritage, reactivation and distribution of fault and fracture network in a rifting context: Case study of the western shoulder of the Upper Rhine Graben. *Journal of Structural Geology,* 108**,** 243-255.

BORGE, H. 2002. Modelling generation and dissipation of overpressure in sedimentary basins: an example from the Halten Terrace, offshore Norway. *Marine and Petroleum Geology,* 19**,** 377-388.

BOWKER, K. A. 2007. Barnett Shale gas production, Fort Worth Basin: Issues and discussion. *Aapg Bulletin,* 91**,** 523-533.

BRüCH, A., GUY, N. & MAGHOUS, S. 2019. Overpressure development in sedimentary basins induced by chemo-mechanical compaction of sandstones. *Marine and Petroleum Geology,* 104**,** 217-230.

CHEN, S., LIU, X., CUI, Y., ZHAO, X. & ZHANG, J. 2017. Palaeogene structural evolution of Dongying Depression, Bohai Bay Basin, NE China. *International Geology Review,* 59**,** 259-273.

CROSSLEY, R. & CROW, M. 1980. The Malawi rift. *Geodynamic Evolution of the Afro-Arabian rift system***,** 78-87.

DOU, L., HOU, J., LIU, Y., ZHANG, L., SONG, S. & WANG, X. 2020. Sedimentary infill of shallow water deltaic sand bodies controlled by small-scale syndepositional faults related paleogeomorphology: Insights from the paleogene Shahejie formation in the Dongying depression, Bohai Bay Basin, Eastern China. *Marine and Petroleum Geology,* 118.

DUGAN, B. & FLEMINGS, P. B. 2000. Overpressure and Fluid Flow in the New Jersey Continental Slope: Implications for Slope Failure and Cold Seeps. *Science,* 289**,** 288-291.

EBINGER, C. J., ROSENDAHL, B. & REYNOLDS, D. 1987. Tectonic model of the Malaŵi rift, Africa. *Tectonophysics,* 141**,** 215-235.

FAULKNER, D. R., JACKSON, C. A. L., LUNN, R. J., SCHLISCHE, R. W., SHIPTON, Z. K., WIBBERLEY, C. A. J. & WITHJACK, M. O. 2010. A review of recent developments concerning the structure, mechanics and fluid flow properties of fault zones. *Journal of Structural Geology,* 32**,** 1557-1575.

FENG, Y., LI, S. & LU, Y. 2013. Sequence stratigraphy and architectural variability in Late Eocene lacustrine strata of the Dongying Depression, Bohai Bay Basin, Eastern China. *Sedimentary Geology,* 295**,** 1-26.

FRERY, E., GRATIER, J.-P., ELLOUZ-ZIMMERMAN, N., LOISELET, C., BRAUN, J., DESCHAMPS, P., BLAMART, D., HAMELIN, B. & SWENNEN, R. 2015. Evolution of fault permeability during episodic fluid circulation: Evidence for the effects of fluid–rock interactions from travertine studies (Utah–USA). *Tectonophysics,* 651-652**,** 121-137.

Gunasekaran, K., DUTTA, J., KUMAR, A., BHARDWAJ, N. & SINHA, N. 2020. Fault-related overpressure in the Krishna-Godavari Basin, India. *Interpretation,* 8**,** T183-T193.

GRAULS, D. J. & BALEIX, J. M. 1994. Role of overpressures and in situ stresses in fault-controlled hydrocarbon migration: a case study. *Marine and Petroleum Geology,* 11**,** 734-742.

GUO, X., HE, S., LIU, K., SONG, G., WANG, X. & SHI, Z. 2010. Oil generation as the dominant overpressure mechanism in the Cenozoic Dongying depression, Bohai Bay Basin, China. *AAPG bulletin,* 94**,** 1859-1881.

GUQIANG, Q., YUN, L. & HONG-HAI, F. 2003. The characteristics and distribution of abnormal pressure in the Paleogene source rocks of Dongying Sag. *Petroleum Exploration and Development,* 30**,** 71-75.

HERON, P. J., PEACE, A. L., MCCAFFREY, K. J. W., WELFORD, J. K., WILSON, R., VAN HUNEN, J. & PYSKLYWEC, R. N. 2019. Segmentation of Rifts Through Structural Inheritance: Creation of the Davis Strait. *Tectonics,* 38**,** 2411-2430.

HOLDSWORTH, B. 2017. Tectonic inheritance, reactivation and long term fault weakening processes.

HSIAO, L.-Y., GRAHAM, S. A. & TILANDER, N. 2004. Seismic reflection imaging of a major strike-slip fault zone in a rift system: Paleogene structure and evolution of the Tan-Lu fault system, Liaodong Bay, Bohai, offshore China. *AAPG Bulletin,* 88**,** 71-97.

HU, S., O'SULLIVAN, P. B., RAZA, A. & KOHN, B. P. 2001. Thermal history and tectonic subsidence of the Bohai Basin, northern China: a Cenozoic rifted and local pull-apart basin. *Physics of the Earth and Planetary Interiors,* 126**,** 221-235.

HUNT, J. M. 1990. Generation and Migration of Petroleum from Abnormally Pressured Fluid Compartments1. *AAPG Bulletin,* 74**,** 1-12.

JACKSON, C. A. L. & ROTEVATN, A. 2013. 3D seismic analysis of the structure and evolution of a salt-influenced normal fault zone: A test of competing fault growth models. *Journal of Structural Geology,* 54**,** 215-234.

LEE, Y. & DEMING, D. 2002. Overpressures in the Anadarko basin,

southwestern Oklahoma: Static or dynamic? *Aapg Bulletin,* 86**,** 145-160.

LI, F. & LI, W. 2017. Petrological record of CO2 influx in the Dongying Sag, Bohai Bay Basin, NE China. *Applied Geochemistry,* 84**,** 373-386.

LI, P.-L. 2004. Oil/gas distribution patterns in Dongying Depression, Bohai Bay Basin. *Journal of Petroleum Science and Engineering,* 41**,** 57-66.

LI, S., ZHAO, G., DAI, L., ZHOU, L., LIU, X., SUO, Y. & SANTOSH, M. 2012. Cenozoic faulting of the Bohai Bay Basin and its bearing on the destruction of the eastern North China Craton. *Journal of Asian Earth Sciences,* 47**,** 80-93.

LI, X., WEI, N., LIU, Y., FANG, Z., DAHOWSKI, R. T. & DAVIDSON, C. L. 2009. CO2 point emission and geological storage capacity in China. *Energy Procedia,* 1**,** 2793-2800.

LI, Z., ZUO, Y., QIU, N. & GAO, J. 2017. Meso–Cenozoic lithospheric thermal structure in the Bohai Bay Basin, eastern North China Craton. *Geoscience Frontiers,* 8**,** 977-987.

LIU, H., JIANG, Y., SONG, G., GU, G., HAO, L. & FENG, Y. 2017. Overpressure characteristics and effects on hydrocarbon distribution in the Bonan Sag, Bohai Bay Basin, China. *Journal of Petroleum Science and Engineering,* 149**,** 811-821.

LIU, Y., QIU, N., YAO, Q., CHANG, J. & XIE, Z. 2016. Distribution, origin and evolution of the Upper Triassic overpressures in the central portion of the Sichuan Basin, SW China. *Journal of Petroleum Science and Engineering,* 146**,** 1116-1129.

LUO, X., DONG, W., YANG, J. & YANG, W. 2003. Overpressuring mechanisms in the Yinggehai Basin, South China Sea. *AAPG Bulletin,* 87**,** 629-645.

MOERNAUT, J., WIEMER, G., REUSCH, A., STARK, N., DE BATIST, M., URRUTIA, R., LADRóN DE GUEVARA, B., KOPF, A. & STRASSER, M. 2017. The influence of overpressure and focused fluid flow on subaquatic slope stability in a formerly glaciated basin: Lake Villarrica (South-Central Chile). *Marine Geology,* 383**,** 35-54.

MUñOZ-BARRERA, J. M., ROTEVATN, A., GAWTHORPE, R. L., HENSTRA, G. A. & KRISTENSEN, T. B. 2020. The role of structural inheritance in the development of high-displacement crustal faults in the necking domain of rifted margins: The Klakk Fault Complex, Frøya High, offshore mid-Norway. *Journal of Structural Geology,* 140.

OMOSANYA, K. D. O. & ALVES, T. M. 2014. Mass-transport deposits controlling fault propagation, reactivation and structural decoupling on continental margins (Espírito Santo Basin, SE Brazil). *Tectonophysics,* 628**,** 158-171.

OSBORNE, M. J. & SWARBRICK, R. E. 1997. Mechanisms for Generating Overpressure in Sedimentary Basins: A Reevaluation1. *AAPG Bulletin,* 81**,** 1023-1041.

PHILLIPS, T. B., A.-L., J. C., BELL, R. E. & DUFFY, O. B. 2018. Oblique reactivation of lithosphere-scale lineaments controls rift physiography - The upper-crustal expression of the Sorgenfrei-Tornquist Zone, offshore southern Norway. *Solid Earth,* 9**,** 403-429.

QIU, N., XU, W., ZUO, Y. & CHANG, J. 2015. Meso–Cenozoic thermal regime in the Bohai Bay Basin, eastern North China Craton. *International Geology Review,* 57**,** 271-289.

RAIMBOURG, H., THIéRY, R., VACELET, M., FAMIN, V., RAMBOZ, C., BOUSSAFIR, M., DISNAR, J.-R. & YAMAGUCHI, A. 2017. Organic matter cracking: A source of fluid overpressure in subducting sediments. *Tectonophysics,* 721**,** 254-274.

REEVE, M. T., BELL, R. E., DUFFY, O. B., JACKSON, A. L. & SANSOM, E. 2015. The growth of non-colinear normal fault systems; What can we learn from 3D seismic reflection data? *Journal of Structural Geology,* 70**,** 141-155.

REN, J., TAMAKI, K., LI, S. & JUNXIA, Z. 2002. Late Mesozoic and Cenozoic rifting and its dynamic setting in Eastern China and adjacent areas. *Tectonophysics,* 344**,** 175-205.

SAMSU, A., CRUDEN, A. R., MICKLETHWAITE, S., GROSE, L. & VOLLGGER, S. A. 2020. Scale matters: The influence of structural inheritance on fracture patterns. *Journal of Structural Geology,* 130.

SCHIFFER, C., DORé, A. G., FOULGER, G. R., FRANKE, D., GEOFFROY, L., GERNIGON, L., HOLDSWORTH, B., KUSZNIR, N., LUNDIN, E., MCCAFFREY, K., PEACE, A. L., PETERSEN, K. D., PHILLIPS, T. B., STEPHENSON, R., STOKER, M. S. & WELFORD, J. K. 2020. Structural inheritance in the North Atlantic. *Earth-Science Reviews,* 206**,** 102975.

ŞENGöR, A. M. C., LOM, N. & SAĞDıç, N. G. 2019. Tectonic inheritance, structure reactivation and lithospheric strength: the relevance of geological history. *Geological Society, London, Special Publications,* 470**,** 105-136.

SEREBRYAKOV, V. A., CHILINGAR, G. V. & KATZ, S. A. 1995. Methods of estimating and predicting abnormal formation pressures. *Journal of Petroleum Science and Engineering,* 13**,** 113-123.

SIBSON, R. H. 1990. Conditions for fault-valve behaviour. *Geological Society, London, Special Publications,* 54**,** 15-28.

SONG, M., LIU, H., WANG, Y. & LIU, Y. 2020. Enrichment rules and exploration practices of Paleogene shale oil in Jiyang Depression, Bohai Bay Basin, China. *Petroleum Exploration and Development,* 47**,** 242-253.

SU, J., ZHU, W., WEI, J., XU, L., YANG, Y., WANG, Z. & ZHANG, Z. 2011. Fault growth and linkage: Implications for tectonosedimentary evolution in the Chezhen Basin of Bohai Bay, eastern China. *AAPG Bulletin,* 95**,** 1-26.

SUWANNASRI, K., PROMRAK, W., UTITSAN, S., CHAISOMBOONPAN, V., GROOT, R. J., SOGNNES, H. I. & MORLEY, C. K. 2014. Reducing the variation of Eaton's exponent for overpressure prediction in a basin affected by multiple overpressure mechanisms. *Interpretation,* 2**,** SB57-SB68.

SWARBRICK, R. & OSBORNE, M. J. 1998. Memoir 70, Chapter 2: Mechanisms that Generate Abnormal Pressures: an Overview.

TARAYOUN, A., MAZZOTTI, S., CRAYMER, M. & HENTON, J. 2018. Structural Inheritance Control on Intraplate Present-Day Deformation: GPS Strain Rate Variations in the Saint Lawrence Valley, Eastern Canada. *Journal of Geophysical Research: Solid Earth*.

TINGAY, M. R., HILLIS, R. R., SWARBRICK, R. E., MORLEY, C. K. & DAMIT, A. R. 2007. 'Vertically transferred'overpressures in Brunei: Evidence for a new mechanism for the formation of high-magnitude overpressure. *Geology,* 35**,** 1023-1026.

TINGAY, M. R. P., HILLIS, R. R., SWARBRICK, R. E., MORLEY, C. K. & DAMIT, A. R. 2009. Origin of overpressure and pore-pressure prediction in the Baram province, Brunei. *AAPG Bulletin,* 93**,** 51-74.

TINGAY, M. R. P., MORLEY, C. K., LAIRD, A., LIMPORNPIPAT, O., KRISADASIMA, K., PABCHANDA, S. & MACINTYRE, H. R. 2013. Evidence for overpressure generation by kerogen-to-gas maturation in the northern Malay Basin. *AAPG Bulletin,* 97**,** 639-672.

WANG, X., HE, S., WEI, A., LIU, Q. & LIU, C. 2016. Typical disequilibrium compaction caused overpressure of Paleocene Dongying Formation in northwest Liaodongwan Depression, Bohai Bay Basin, China. *Journal of Petroleum Science and Engineering,* 147**,** 726-734.

WANG, Y., CHANG, X., SUN, Y., SHI, B. & QIN, S. 2020. Timeframe of hydrocarbon migration in the Paleogene Shahejie Formation in the Dongying depression, Bohai Bay Basin (northeastern China) based on fluid inclusions and oil geochemistry. *Journal of Petroleum Science and Engineering,* 193.

WATSON, M. P., HAYWARD, A. B., PARKINSON, D. N. & ZHANG, Z. M. 1987. Plate tectonic history, basin development and petroleum source rock deposition onshore China. *Marine and Petroleum Geology,* 4**,** 205-225.

WEDMORE, L. N. J., WILLIAMS, J. N., BIGGS, J., FAGERENG, Å., MPHEPO, F., DULANYA, Z., WILLOUGHBY, J., MDALA, H. & ADAMS, B. A. 2020. Structural inheritance and border fault reactivation during active early-stage rifting along the Thyolo fault, Malawi. *Journal of Structural Geology,* 139**,** 104097.

WILSON, J. T. 1966. Did the Atlantic Close and then Re-Open? *Nature,* 211**,** 676-681.

WIPRUT, D. & ZOBACK, M. D. 2000. Fault reactivation and fluid flow along a previously dormant normal fault in the northern North Sea. *Geology,* 28**,** 595-598.

XIAORONG, LUO, WEILIANG, DONG, JIHAI, YANG, WAN & YANG 2003. Overpressuring mechanisms in the Yinggehai Basin, South China Sea. *Aapg Bulletin,* 87**,** 629-645.

YANG, W., PENG, B., LIU, Q., WANG, S., DONG, Y. & LAI, Y. 2017. Evaluation of CO 2 enhanced oil recovery and CO 2 storage potential in oil reservoirs of Bohai Bay Basin, China. *International Journal of Greenhouse Gas Control,* 65**,** 86-98.

YARDLEY, G. S. & SWARBRICK, R. E. 2000. Lateral transfer: a source of additional overpressure? *Marine and Petroleum Geology,* 17**,** 523-537.

YOU, B., NI, Z., ZENG, J., LUO, Q., XIAO, H., SONG, G. & WANG, Y. 2020. Oil-charging history constrained by biomarkers of petroleum inclusions in the Dongying Depression, China. *Marine and Petroleum Geology,* 122.

ZAHID, M. A., CHUNMEI, D., LIN, C., GLUYAS, J., JONES, S., ZHANG, X., MUNAWAR, M. J. & MA, C. 2016. Sequence stratigraphy, sedimentary facies and reservoir quality of Es4s, southern slope of Dongying Depression, Bohai Bay Basin, East China. *Marine and Petroleum Geology,* 77**,** 448-470.
ZE, T. & ALVES, T. M. 2016. The role of gravitational collapse in controlling the evolution of crestal fault systems (Espírito Santo Basin, SE Brazil). *Journal of Structural Geology,* 92**,** 79-98.
ZE, T. & ALVES, T. M. 2019. Impacts of data sampling on the interpretation of normal fault propagation and segment linkage. Tectonophysics, 762, 79-96.
ZHANG, L., LIU, Q., ZHU, R., LI, Z. & LU, X. 2009. Source rocks in Mesozoic–Cenozoic continental rift basins, east China: A case from Dongying Depression, Bohai Bay Basin. *Organic Geochemistry,* 40**,** 229-242.

Figure Captions

Figure 1. Location of the study area. a) Location of the Bohai Bay Basin and related sub-basins. The Dongying depression is located in the southern part of the Jiyang sub-basin. 2) Seismic and well data used in the study. Black boxes show locations of the two seismic cubes used in the study area.

Figure 2. Regional structural sections. a) Regional cross sections of the Bohai Bay Basin (modified from Li et al., 2012). Present-day structural divisions of the Bohai Bay Basin show distinct differences between western and eastern parts. In the southeast, steep faults that root onto the Moho controlled its structural evolution, while in the northwest, slip-dip faults were developed. In the study area, Paleogene strata laid directly on top of the Neoproterozoic basement. b) Structural section of the Dongying depression (modified after Wang et al., 2020).

Figure 3. Generalized Cenozoic–Quaternary stratigraphic framework showing tectonic and sedimentary evolution stages and the major petroleum system elements of the Dongying depression, Bohai, Bay Basin, East China (Modified after Guo et. al., 2012). Two stages of evolution since the Paleocene were identified: syn-rift stage (65.0–24.6 Ma) and post-rift stage (24.6 Ma to the present). The Paleogene syn-rift stage can be further divided in to four stages as follows: 1) an early-initial rifting from Paleocene to early Eocene (65–50.4 Ma), 2) a late rifting in the Middle Eocene (50.4–42.5 Ma), 3) a rift climax from the late Eocene to early Oligocene (42.5–38 Ma), and 4) weakened rifting during Oligocene (38–24.6 Ma). Three sets of main hydrocarbon source intervals in the Paleogene Shahejie Formation, namely the upper Es4, the lower Es3 and the upper Es3 members were developed, which also constitutes the main oil producing intervals in the Dongying depression.

Figure 4. Seismic section showing faults developed in the Lijin Sag. Five groups of faults were identified in the Lijin Sag as follows: 1) the Shengtuo Fault, which strikes along the E–W direction and stretches onto the basement in the Lijin sag, comprising the border fault in the Lijin sag, 2) faults formed during syn-rift stage 1, which offset the Paleocene Kongdian strata, 3) faults developed during syn-rift stage 3 (H2 and H3), which offset the overlying strata during the later stages of their evolution, 4) tier-bound faults, faults that were developed during syn-rift stage 3 and are bounded by horizons H3 and H4, and 5) faults that were formed during the post-rift stage, revealing maximum throw values at horizons H6.

Figure 5. Variance maps at different depths showing fault groups in the Lijin Sag. a) Variance map between horizons H3 and H4 show that Fault Family 2 was formed during syn-rift stages 1 and 2 and did not propagate into this interval. b) Variance map imaging strata deposited during syn-rift stage 3 shows the development of Fault Family 4. c) Variance map imaging a stratigraphic level between syn-rift stages 3 and 4 revealing that Fault Family 4 scarcely propagated into the overlying strata. d) Variance map of strata in syn-rift stage 4 revealing the distribution of Fault Family 5. We stress that faults developed during syn-rift stages 3 and 4 are rarely linked. Other significant faults include: 1) the Shengtuo fault, which constitutes the border fault in the study area, and 2) Fault Family 2, which offsets strata deposited during syn-rift stage 3.

Figure 6. Seismic section imaging faults developed in the Boxing Sag. Three phases of faulting can be identified as: phase 1) faulting occurred during syn-rift stages 1 and 2 (spanning the basement to

horizon H2), phase 2) recording the reactivation of phase 1 faults, and 3) further fault propagation and reactivation at the level of horizon H6.

Figure 7. Variance maps at different depths imaging the importance of structural inheritance in the Boxing Sag. a) Intensive faulting during syn-rift stages 1 and 2. b) Reactivation of pre-existing faults, which propagated upwards forming fault systems in syn-rift stage 3 strata. c) Reactivation of pre-existing faults, which propagated upwards forming fault systems in syn-rift stage 4 strata.

Figure 8. Throw-depth (T-Z) plots of distinct faults in the Boxing Sag. For the five faults analyzed, dramatic increases in throw values are observed at horizon H2 or below, indicating faulting during syn-rift stages 1 and 2. Apart from the three main phases of faulting documented in the Boxing sag, which were separated by two regional unconformities (horizons H2 and H6), other fault reactivation periods are highlighted in the T-Z plots. Faults B4 presents a phase of fault reactivation during syn-rift stage 4 (horizon H4), and fault B2 shows a phase of fault reactivation during the post-rift stage (horizon H7).

Figure 9. Seismic-borehole tie highlighting the pressure coefficient estimated in the Lijin Sag. Pressure coefficient from three wells in the Lijin sag, T140, T719 and T710, were recorded in the Es_4 member. Four wells (T714, T 712, T71, and T711) recorded pressure coefficients in the Es_3 member. In the Es4 member, the pressure coefficient is 1.77 in well T140, which is categorized as a well with high overpressure. In wells T719 and T710, pressure coefficients are 1.19 and 1.29, respectively, identified as low to moderate overpressures. Normal pore pressure with a pressure coefficient of 0.85 occurs in the Es_3 member in well T711. Other wells show high overpressures in the Es_3 member, with pressure coefficients of 1.70 in well T714, 1.68 in well T712, and 1.86 in well T71. When approaching Fault L1 in the study area, which offset strata from the basement to the surface, pore pressure declines dramatically.

Figure 10. Seismic-borehole tie highlighting the pressure coefficient estimated in the Lijin Sag. Pressure coefficients for seven wells in the Boxing sag are estimated in the Es_4 member (red dots), while pressure coefficients from four wells are recorded in the Es_3 member (blue dots). In the Es_4 member, normal pore pressure is observed in well Tg85 (pressure coefficient=1.09), which is located on the hanging wall of Fault B3. High overpressures are developed in well L109, with a pressure coefficient of 1.54. Other wells show low to moderate overpressure in the Es_4 member, with pressure coefficients of 1.26 in well Tg81, 1.14 in well Ch97, 1.33 in well Ch96, 1.26 in well Ch69, and 1.18 in well L5, respectively. In the Es_3 member, wells Ch60 and Ch38 show normal pore pressure with coefficients of 0.95 and 1.09, respectively. Wells Ch106 and Tg84 indicate moderate overpressure magnitude.

Figure 11. LWD pore pressures in the Lijin and Boxing sags. A) Overall pore-pressure coefficient statistics. Pressure coefficient varies from 0.90 to 1.92 in the Lijin sag, with 36 wells showing normal pore pressures, 28 wells have low to moderate pore pressure, and 26 wells have high pressure coefficients in the Es_3 and Es_4 members. In the Boxing Sag, pressure coefficients vary from 0.91 to 1.54 (Fig. 11a). Thirty-one (31) wells show normal pore pressure at present, eighty-one (88) wells have low to moderate overpressure being developed, and one well show high pressure coefficients of 1.54 in the Es4 member. b) Overall pore pressure coefficients for the Es_4 member. Results show that 16 wells with normal pore pressure, 9 wells with low overpressure, and 58 wells with moderate overpressure are documented in the Boxing sag (Fig. 11b). In the Lijin Sag, 10 wells have normal pore pressure, 9 wells developed moderate overpressure, and 11 wells have high overpressure. c) Overall pore pressure coefficients statistics in the Es_3 member. Six wells, of a total of 14 wells, show low to moderate overpressures in the Boxing Sag, and 28 wells out of 47 wells show moderate to high overpressures in the Lijin Sag.

Figure 12. Control of structural inheritance on overpressure development in the study area. Two end members of faulting in sedimentary basins, the Lijin and the Boxing types, are proposed according to the effect of border faults on overpressure development. During stage 1, both sags experienced intensive rifting in syn-rift stages 1 and 2 and numerous faults were formed (a and a'). The Shengtuo Fault was established as a border fault during stage 2. Scarce new faults were formed in the younger strata (b). In the Boxing sag, fault reactivation dominated the faulting styles in the younger strata, and no border faults are considered to have formed during stage 2 (b'). With continuous sedimentation, shale/mudstones reached hydrocarbon generation depths, leading to the accumulation of overpressure in both sags (c and c'). In the Lijin Sag new faults were formed in younger strata, which were not connected with faults that formed during stage 1 (c). Leakage of fluids along the border faults and newly generated faults occurred in the Lijin Sag, leading to a decline of pressure in the reservoir successions (c). In the Boxing sag, a new phase of fault reactivation occurred, inducing the systematic release of fluid from source and reservoir intervals into younger strata or the surface, inducing a decline in pore pressure greater than that in the Lijin Sag (c'). During the post-rift stage, new faults were generated in the Lijin Sag, and these were not linked with faults formed during previous stages, i.e. the main petroleum systems were not faulted (d). Continuous oil generation and oil-gas cracking enhanced pore pressure in the hydrocarbon-productive units of the Lijin Sag. In the Boxing Sag, post-rift faulting resulted in the fault reactivation of pre-existing faults. Faults at all stratigraphic units were reactivated, leading to further pore pressure decline in reservoirs succession (d').

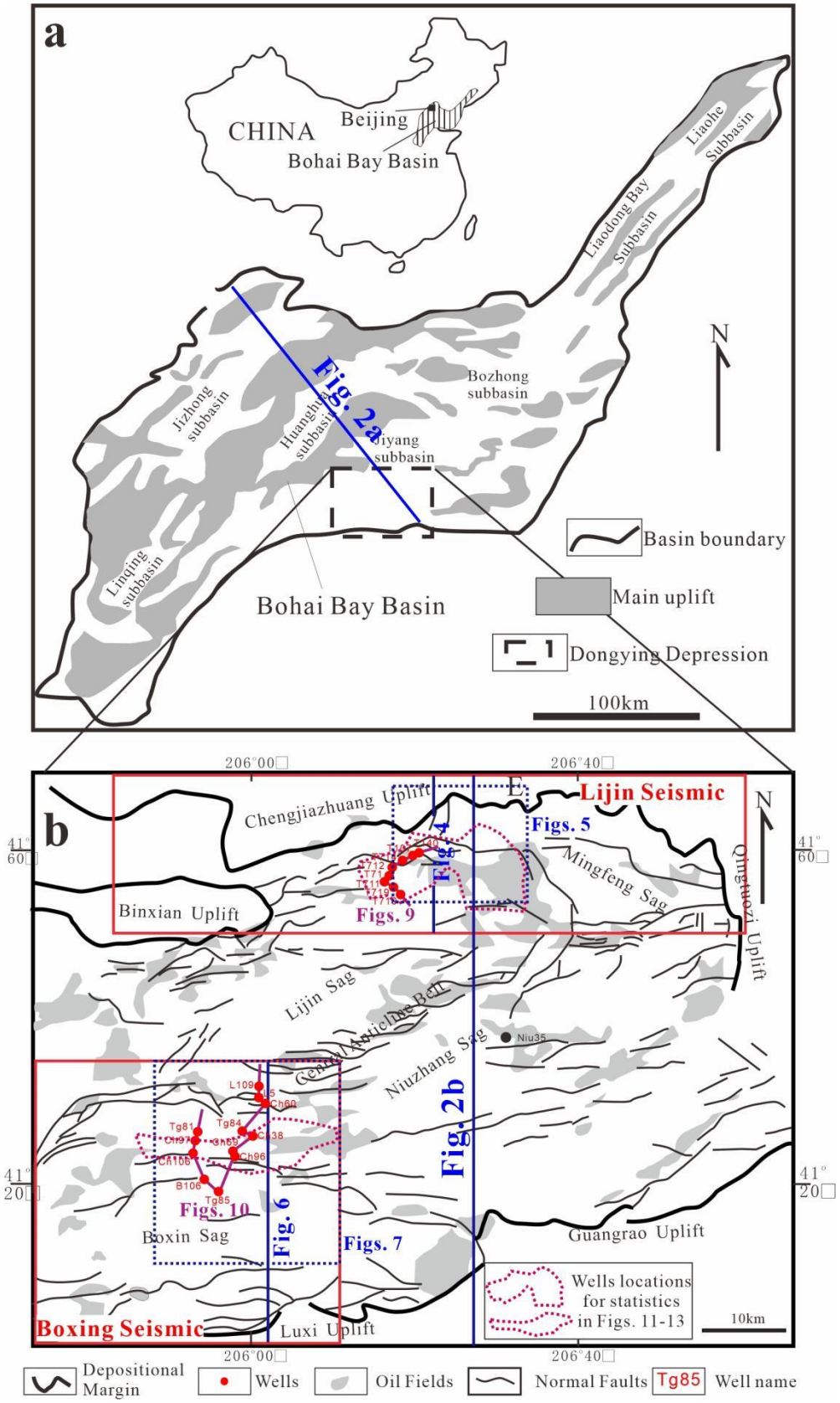
a
CHINA
Beijing
Bohai Bay Basin
Liaohe Subbasin
Liaodong Bay Subbasin
Bozhong subbasin
Jizhong subbasin
Huanghua subbasin
Qiyang subbasin
Linqing subbasin
Fig. 2a
N
Basin boundary
Main uplift
Dongying Depression
100km
Bohai Bay Basin
b
206°00
206°40
41° 60
41° 20
Chengjiazhuang Uplift
Lijin Seismic
Figs. 5
Figs. 4
Figs. 9
Mingfeng Sag
Qingtuozi Uplift
Binxian Uplift
Lijin Sag
Central Anticline Belt
Niuzhang Sag
Niu35
Fig. 2b
Figs. 10
Boxin Sag
Fig. 6
Figs. 7
Guangrao Uplift
Boxing Seismic
Luxi Uplift
Wells locations for statistics in Figs. 11-13
10km
Depositional Margin
Wells
Oil Fields
Normal Faults
Tg85
Well name

Figure 1

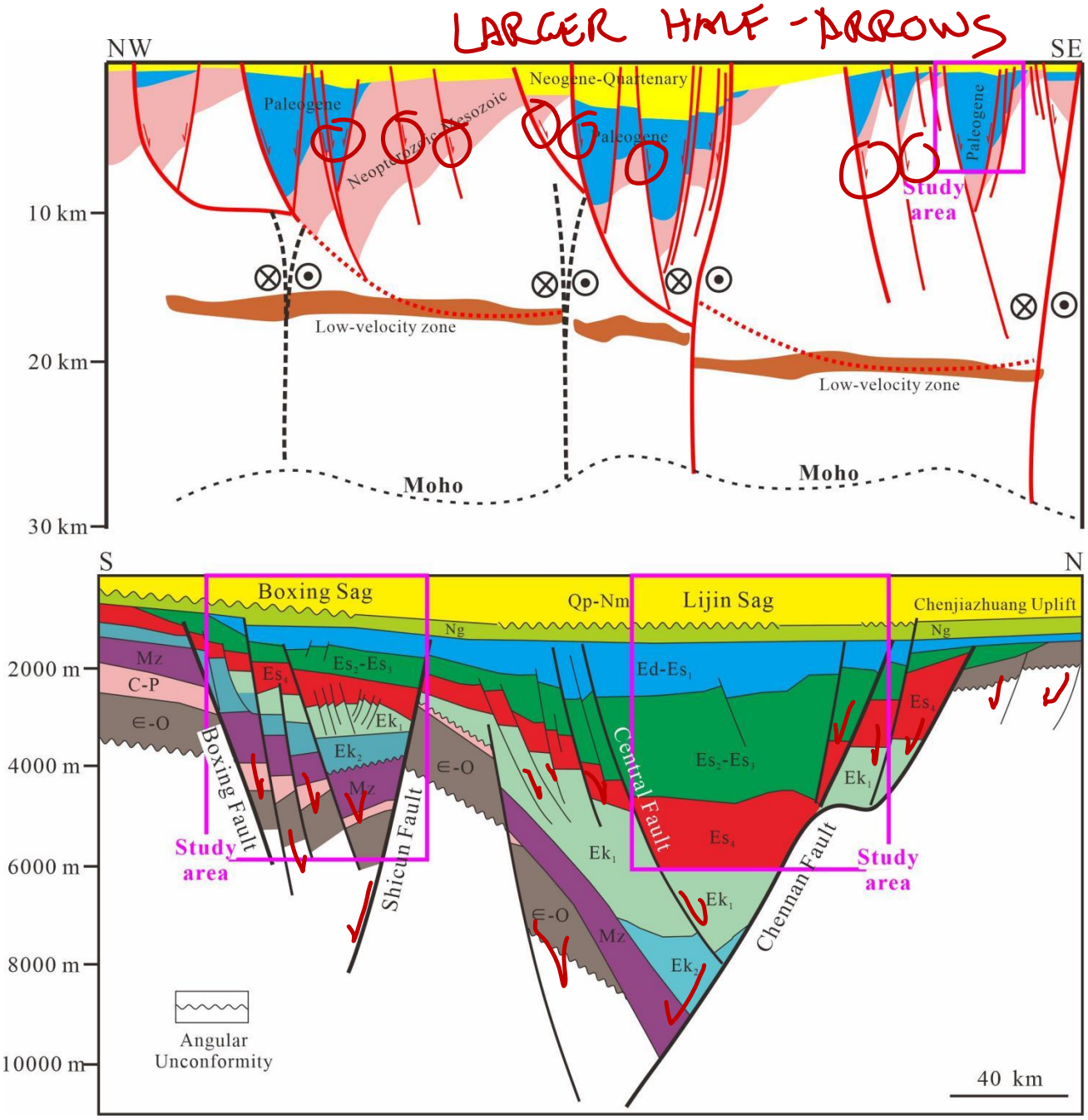
LARGER HMF - ARROWS
NW
SE
Neogene-Quartenary
Paleogene
Neoproterozoic-Mesozoic
Paleogene
Paleogene
Study area
10 km
20 km
30 km
Low-velocity zone
Low-velocity zone
Moho
Moho
S
N
Boxing Sag
Qp-Nm
Lijin Sag
Chenjiazhuang Uplift
Ng
Ng
Mz
C-P
∈-O
Es4
Es2-Es3
Ek1
Ek2
Mz
∈-O
Boxing Fault
Shicun Fault
Central Fault
Ed-Es1
Es2-Es3
Es4
Ek1
Ek1
∈-O
Mz
Ek2
Chennan Fault
Study area
Study area
2000 m
4000 m
6000 m
8000 m
10000 m
Angular Unconformity
40 km

Figure 2

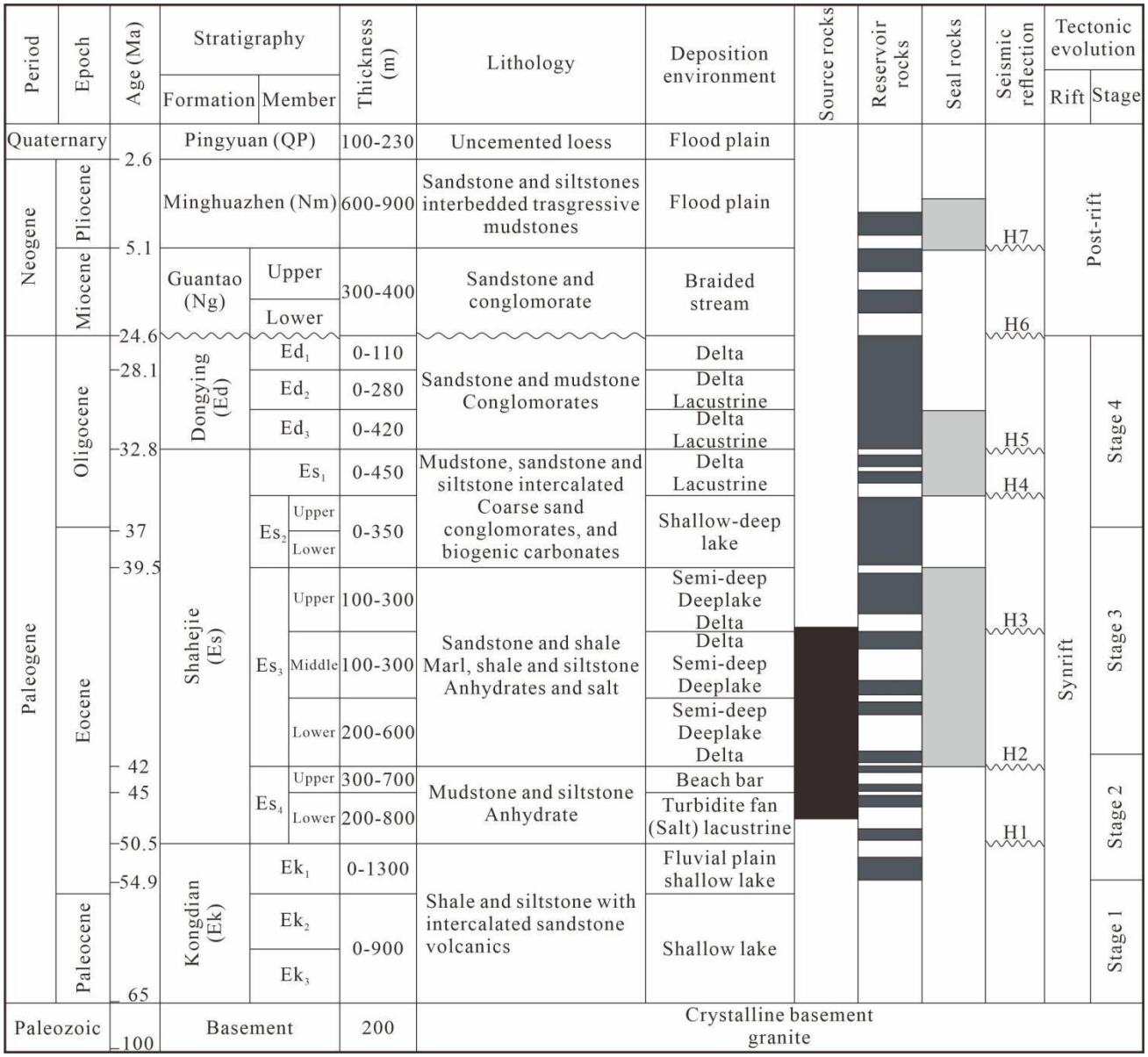
Period
Epoch
Age (Ma)
Stratigraphy
Formation
Member
Thickness (m)
Lithology
Deposition environment
Source rocks
Reservoir rocks
Seal rocks
Seismic reflection
Tectonic evolution
Rift
Stage
Quaternary
Pingyuan (QP)
100-230
Uncemented loess
Flood plain
Neogene
Pliocene
2.6
Minghuazhen (Nm)
600-900
Sandstone and siltstones interbedded trasgressive mudstones
Flood plain
H7
Post-rift
Miocene
5.1
Guantao (Ng)
Upper
Lower
300-400
Sandstone and conglomorate
Braided stream
H6
24.6
Paleogene
Oligocene
28.1
Dongying (Ed)
Ed1
0-110
Sandstone and mudstone Conglomorates
Delta
Synrift
Stage 4
Ed2
0-280
Delta Lacustrine
Ed3
0-420
Delta Lacustrine
32.8
H5
Shahejie (Es)
Es1
0-450
Mudstone, sandstone and siltstone intercalated Coarse sand conglomorates, and biogenic carbonates
Delta Lacustrine
H4
Es2
Upper
Lower
0-350
Shallow-deep lake
Eocene
37
39.5
Es3
Upper
100-300
Sandstone and shale Marl, shale and siltstone Anhydrates and salt
Semi-deep Deeplake Delta
H3
Stage 3
Middle
100-300
Delta Semi-deep Deeplake
Lower
200-600
Semi-deep Deeplake Delta
H2
42
Es4
Upper
300-700
Mudstone and siltstone Anhydrate
Beach bar
Stage 2
45
Lower
200-800
Turbidite fan (Salt) lacustrine
50.5
H1
Kongdian (Ek)
Ek1
0-1300
Shale and siltstone with intercalated sandstone volcanics
Fluvial plain shallow lake
54.9
Paleocene
Ek2
0-900
Shallow lake
Stage 1
Ek3
65
Paleozoic
100
Basement
200
Crystalline basement granite

Figure 3

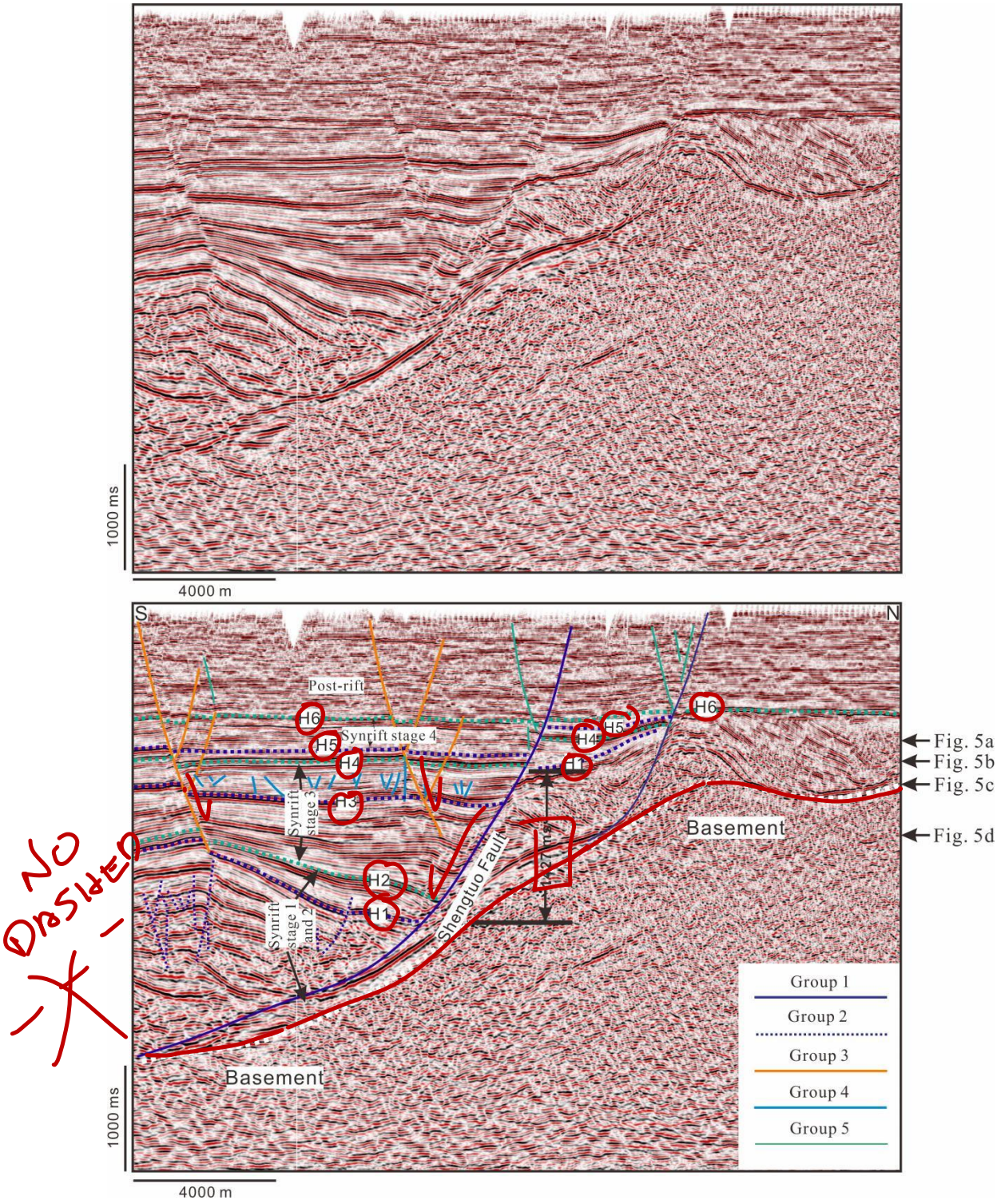
1000 ms
4000 m
S
N
Post-rift
Synrift stage 4
Synrift stage 3
Synrift stage 1 and 2
H1
H2
H3
H4
H5
H6
Shengtuo Fault
Basement
Basement
Fig. 5a
Fig. 5b
Fig. 5c
Fig. 5d
Group 1
Group 2
Group 3
Group 4
Group 5
1000 ms
4000 m

Figure 4

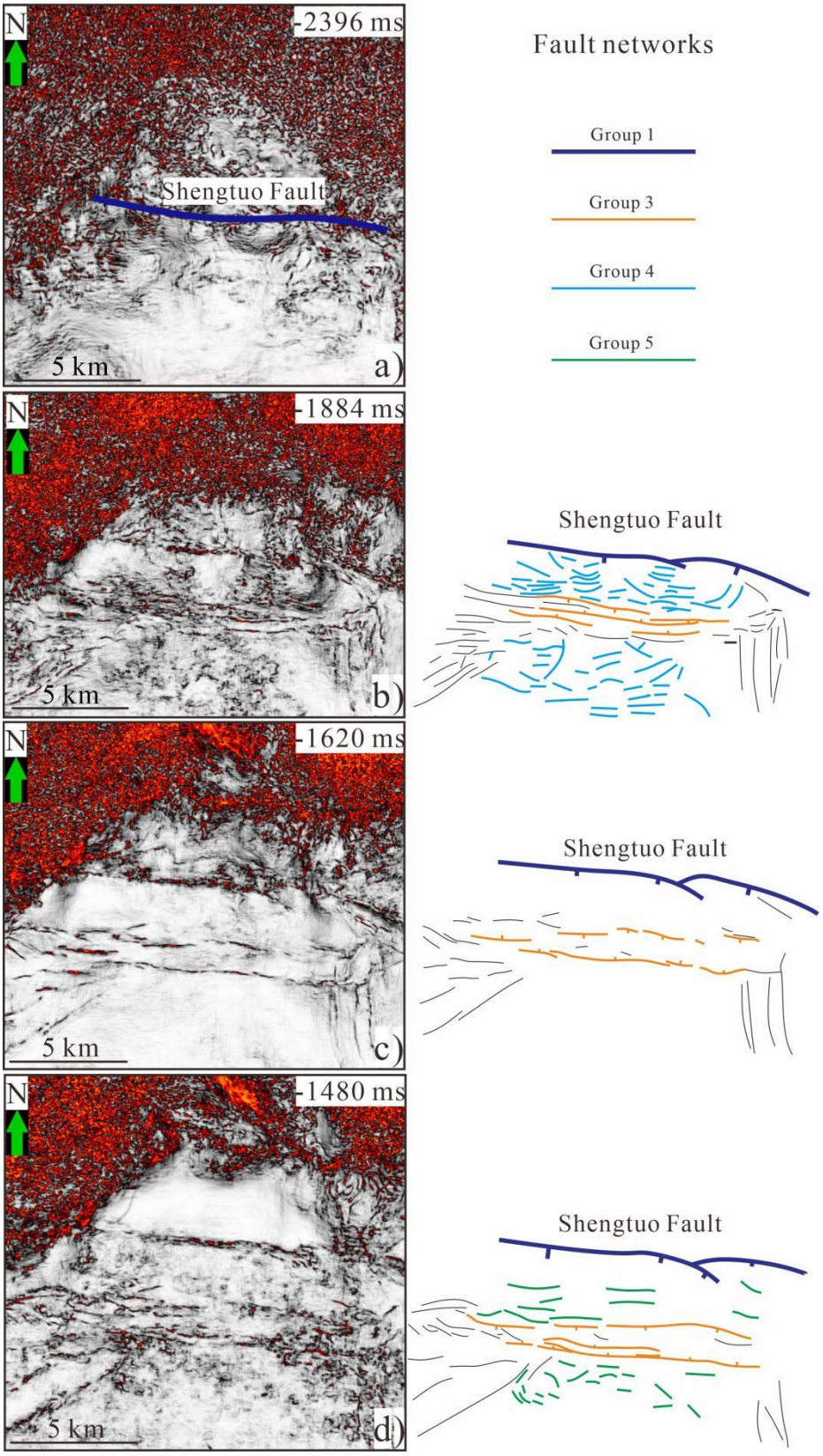
N
-2396 ms
Shengtuo Fault
5 km
a)
Fault networks
Group 1
Group 3
Group 4
Group 5
N
-1884 ms
5 km
b)
Shengtuo Fault
N
-1620 ms
5 km
c)
Shengtuo Fault
N
-1480 ms
5 km
d)
Shengtuo Fault

Figure 5

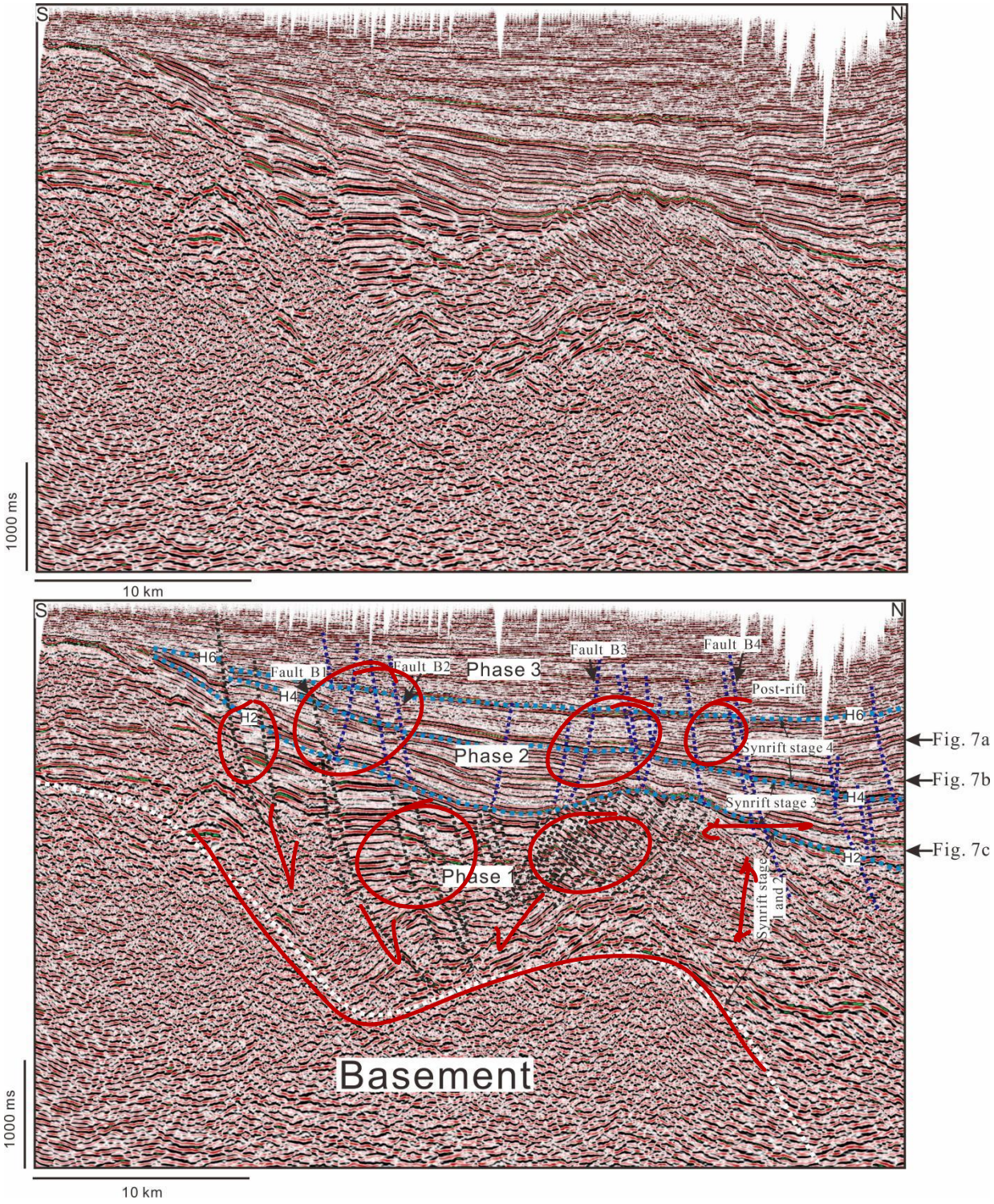
S
N
1000 ms
10 km
S
N
H6
Fault_B1
H4
H2
Fault_B2
Phase 3
Fault_B3
Fault_B4
Post-rift
H6
Synrift stage 4
Phase 2
Synrift stage 3
H4
H2
Phase 1
Synrift stage 1 and 2
Basement
Fig. 7a
Fig. 7b
Fig. 7c
1000 ms
10 km

Figure 6

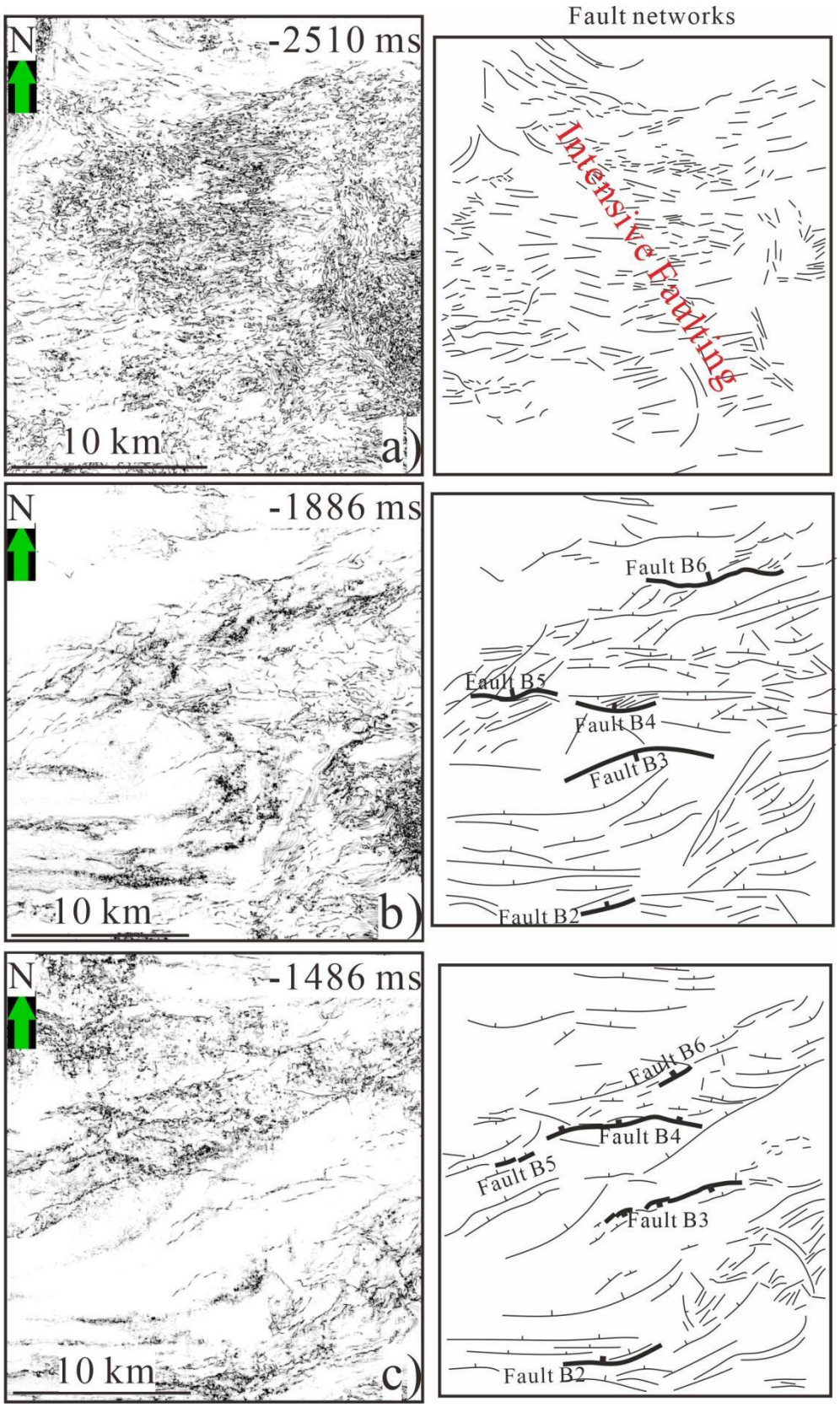
Fault networks
N
-2510 ms
10 km
a)
Intensive Faulting
N
-1886 ms
10 km
b)
Fault B6
Fault B5
Fault B4
Fault B3
Fault B2
N
-1486 ms
10 km
c)
Fault B6
Fault B4
Fault B5
Fault B3
Fault B2

Figure 7

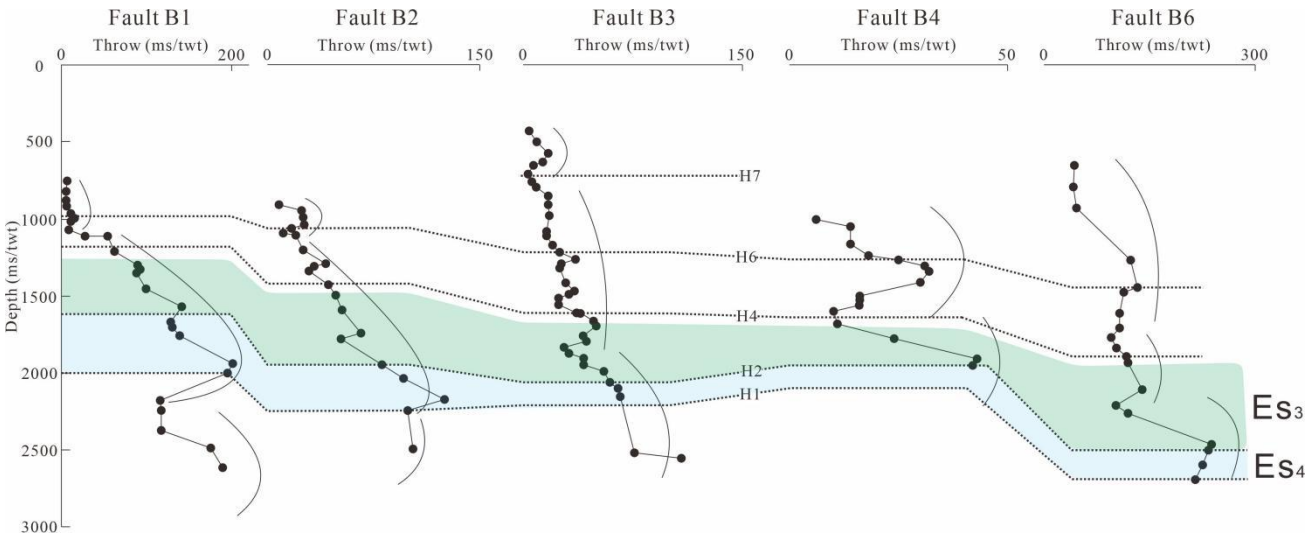

Figure 8

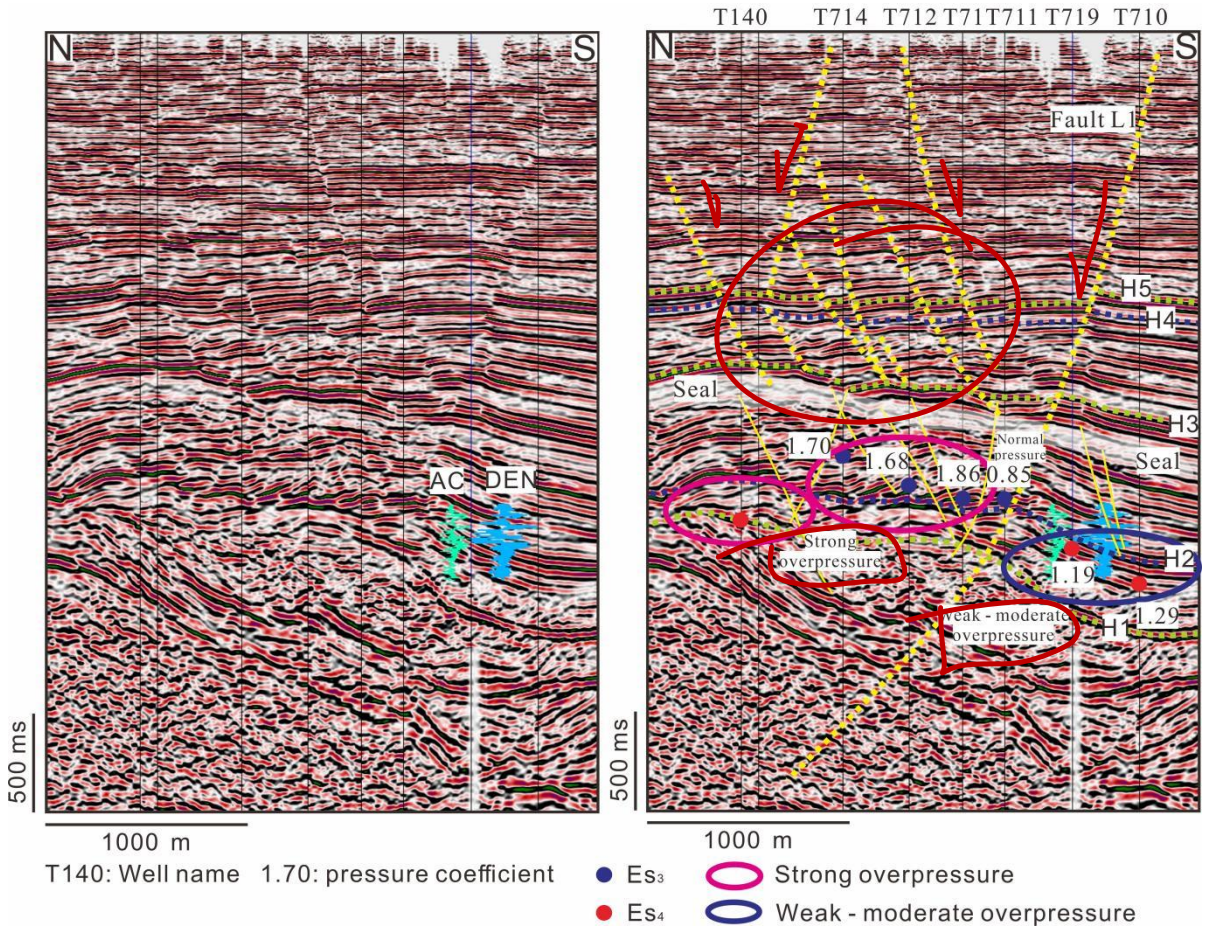

Figure 9

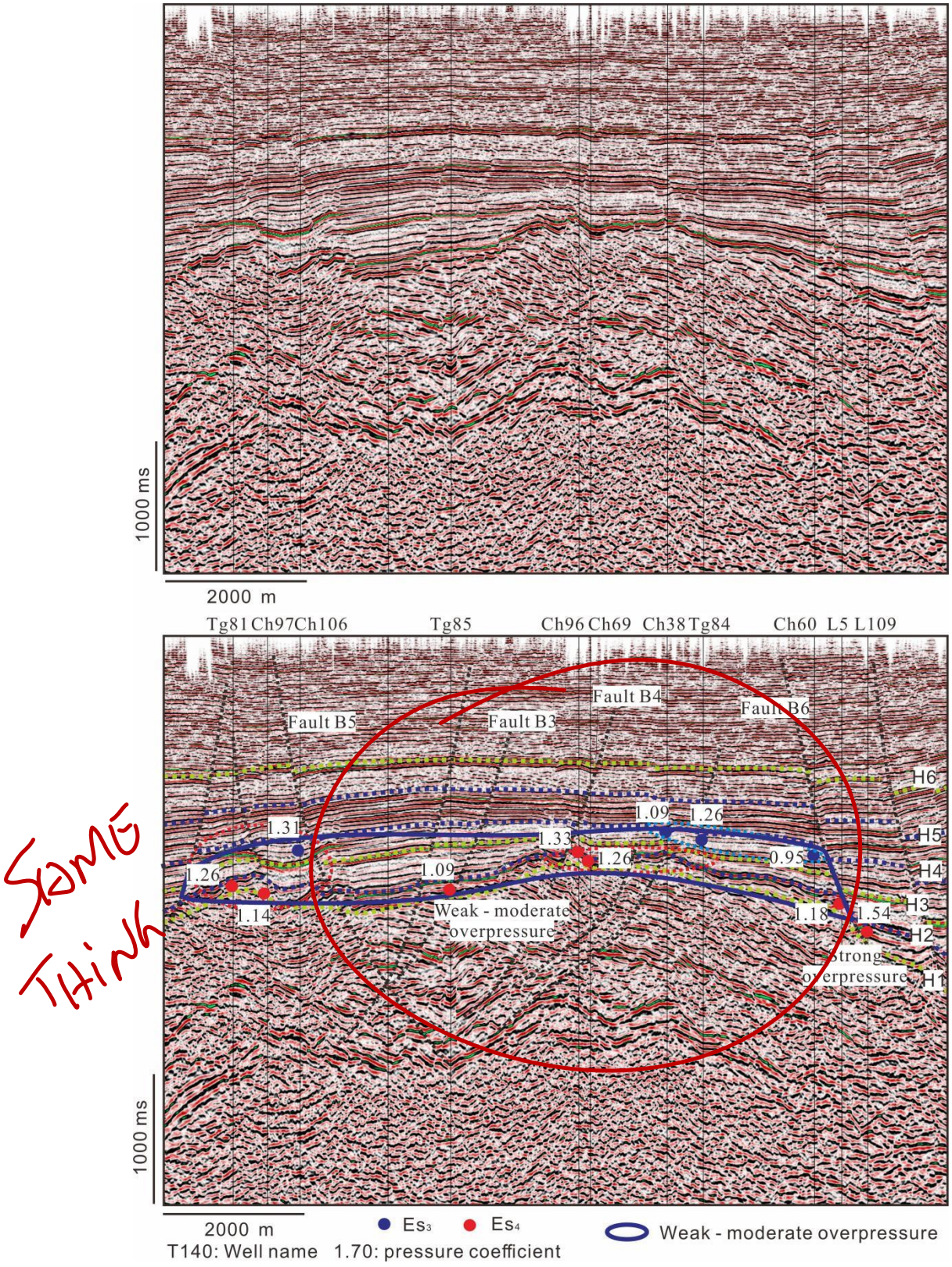
1000 ms
2000 m
Tg81 Ch97Ch106
Tg85
Ch96 Ch69 Ch38 Tg84
Ch60 L5 L109
Fault B5
Fault B3
Fault B4
Fault B6
H6
H5
H4
H3
H2
H1
1.31
1.26
1.14
1.09
1.33
1.26
1.09
1.26
0.95
1.18
1.54
Weak - moderate overpressure
Strong overpressure
1000 ms
2000 m
Es3
Es4
Weak - moderate overpressure
T140: Well name 1.70: pressure coefficient

Figure 10

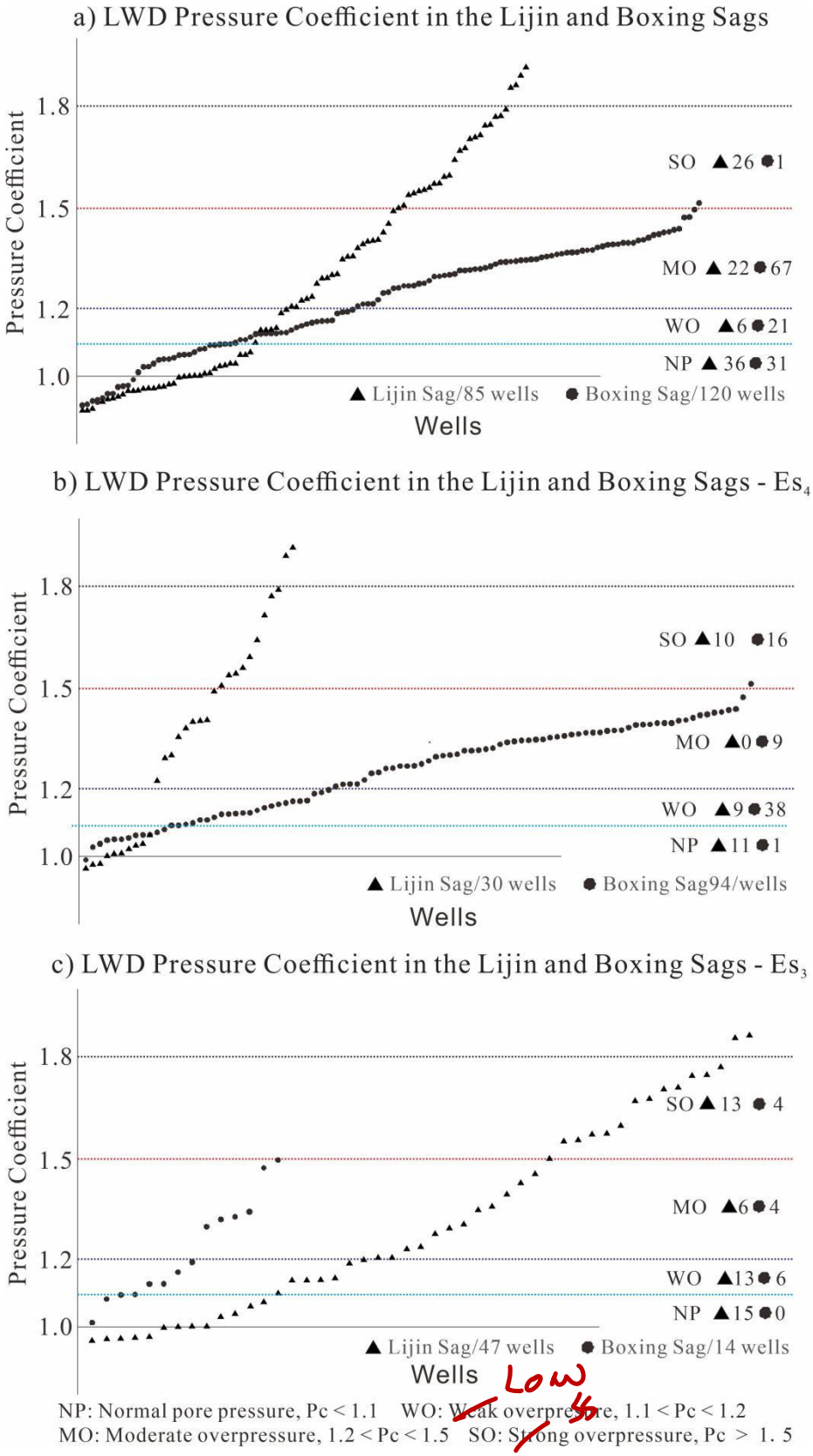
a) LWD Pressure Coefficient in the Lijin and Boxing Sags
Pressure Coefficient
1.8
1.5
1.2
1.0
SO ▲26 ●1
MO ▲22 ●67
WO ▲6 ●21
NP ▲36 ●31
▲ Lijin Sag/85 wells ● Boxing Sag/120 wells
Wells
b) LWD Pressure Coefficient in the Lijin and Boxing Sags - Es4
Pressure Coefficient
1.8
1.5
1.2
1.0
SO ▲10 ●16
MO ▲0 ●9
WO ▲9 ●38
NP ▲11 ●1
▲ Lijin Sag/30 wells ● Boxing Sag94/wells
Wells
c) LWD Pressure Coefficient in the Lijin and Boxing Sags - Es3
Pressure Coefficient
1.8
1.5
1.2
1.0
SO ▲13 ● 4
MO ▲6 ●4
WO ▲13 ●6
NP ▲15 ●0
▲ Lijin Sag/47 wells ● Boxing Sag/14 wells
Wells
NP: Normal pore pressure, Pc < 1.1 WO: Weak overpressure, 1.1 < Pc < 1.2
MO: Moderate overpressure, 1.2 < Pc < 1.5 SO: Strong overpressure, Pc > 1. 5

Figure 11

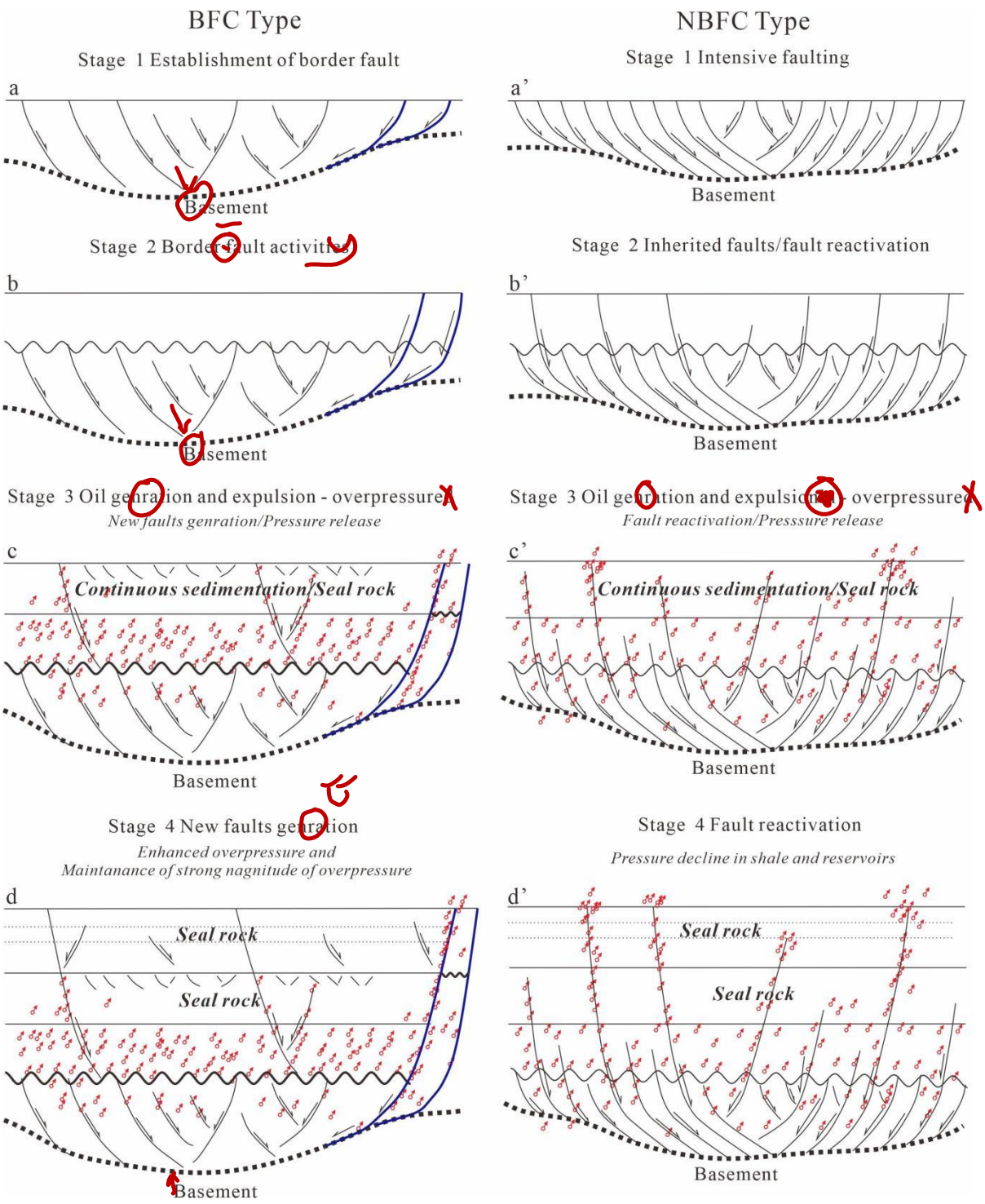
BFC Type
Stage 1 Establishment of border fault
a
Basement
Stage 2 Border fault activities
b
Basement
Stage 3 Oil genration and expulsion - overpressured
New faults genration/Pressure release
c
Continuous sedimentation/Seal rock
Basement
Stage 4 New faults genration
Enhanced overpressure and
Maintanance of strong nagnitude of overpressure
d
Seal rock
Seal rock
Basement
NBFC Type
Stage 1 Intensive faulting
a'
Basement
Stage 2 Inherited faults/fault reactivation
b'
Basement
Stage 3 Oil genration and expulsion - overpressured
Fault reactivation/Presssure release
c'
Continuous sedimentation/Seal rock
Basement
Stage 4 Fault reactivation
Pressure decline in shale and reservoirs
d'
Seal rock
Seal rock
Basement

Figure 12